General-mass treatment for deep inelastic scattering at two-loop accuracy

Marco Guzzi, Pavel M. Nadolsky, Hung-Liang Lai, and C.-P. Yuan

General-mass treatment for deep inelastic scattering
at two-loop accuracy

Marco Guzzi,[1] Pavel M. Nadolsky,[1] Hung-Liang Lai,[2] C.-P. Yuan[3,4]

[1]*Department of Physics,*

Southern Methodist University,

Dallas, TX 75275, USA

[2]*Taipei Municipal University of Education,*

Taipei, Taiwan

[3]*Department of Physics & Astronomy,*

Michigan State University,

East Lansing, MI 48824, USA

[4]*Center for High Energy Physics,*

Peking University, Beijing 100871, China

We present a next-to-next-to-leading order (NNLO) realization of a general quark mass scheme (S-ACOT-χ) in deep inelastic scattering and explore the impact of NNLO terms on heavy-quark structure functions $F_{2,L}^c(x,Q)$. An amended QCD factorization theorem for DIS is discussed that validates the S-ACOT-χ scheme to all orders in the QCD coupling strength. As a new feature, kinematical constraints on collinear production of heavy quarks that are crucial near the heavy-quark threshold are included in the amended factorization theorem. An algorithmic procedure is outlined for implementing this scheme at NNLO by using mass-dependent and massless results from literature. At two loops in QCD cut diagrams, the S-ACOT-χ scheme reduces scale dependence of heavy-quark DIS cross sections as compared to the fixed-flavor number scheme.

I. INTRODUCTION

In a modern global QCD analysis of parton distribution functions (PDFs), several factors are comparable in magnitude to next-to-next-to-leading order (NNLO) radiative contributions in the QCD coupling strength α_s. Among these factors, dependence of QCD cross

sections on masses of heavy quarks, m_c and m_b, can be significant. Global fits are sensitive to two types of mass effects, kinematical suppression of production of c and b quarks near respective mass thresholds in deep inelastic scattering (DIS), and large radiative contributions to collinear production of $c\bar{c}$ or $b\bar{b}$ pairs at large collider energy. The first effect – suppression of DIS charm production near the threshold – must be carefully estimated when obtaining PDF parametrizations in order to accurately predict key scattering rates at the Large Hadron Collider [1]. The second effect is tied to an observation that c and b quarks behave as practically massless and indistinguishable from other massless flavors in typical Tevatron and LHC observables. It is therefore natural to evaluate all fitted cross sections in a "general-mass" (GM) factorization scheme, which assumes that the number of (nearly) massless quark flavors varies with energy, and at the same time includes dependence on heavy-quark masses in relevant kinematical regions.

In this paper, we study NNLO quark mass terms in the default GM scheme of CTEQ PDF analyses called "S-ACOT-χ". Here and in the following, the order of the calculation is defined by the number of QCD loops in Feynman cut diagrams, so that "NNLO" refers to the two-loop accuracy, or $\mathcal{O}(\alpha_s^2)$, in the DIS coefficient functions. Since its inception in 1993 [2], the ACOT scheme has undergone evolution based on the work in [3–5]. The S-ACOT-χ version of the ACOT scheme is employed successfully to compute heavy-quark cross sections in recent NLO CTEQ6.6, CT09, and CT10 global fits [6–8].

The S-ACOT-χ scheme is motivated by the QCD factorization theorem for DIS with massive quarks [3], which provides the scheme's organizational backbone and key methods. In Sec. II, we demonstrate how to amend the QCD factorization theorem in order to validate the S-ACOT-χ scheme to all orders of α_s. We then apply this scheme at NNLO to neutral-current DIS production, which provides the bulk of the DIS data, and for which all components of the calculation are readily available.[1]

Compared to other heavy-quark schemes available at NNLO [12–18], our implementation aims to achieve more explicit analogy to the computation of NNLO cross sections in the zero-mass (ZM) scheme [19–21]. As another distinction, the S-ACOT-χ scheme quickly converges to the fixed-flavor number scheme near the heavy-quark threshold as a consequence of the

---

[1] For charged-current DIS, only massless [9, 10] and some massive [11] NNLO coefficient functions have been computed.

amended factorization theorem, without requiring supplemental matching conditions that are present in other general-mass schemes.

In Sec. II, the S-ACOT-χ cross sections are presented in the form that is reminiscent of counterpart ZM cross sections, up to replacement of some massless components by their mass-dependent expressions available in literature. This representation is based on a few compact formulas that include the desirable features existing in other heavy-quark NNLO calculations. In Sec. III, numerical predictions are illustrated on the example of NNLO charm production cross sections. They show that inclusion of the NNLO terms reduces theoretical uncertainties compared to NLO.

Recent studies [1, 22–24] show that, at NLO, the LHC electroweak cross sections depend considerably on the mass scheme and parametric input for the charm mass m_c in the PDF analysis, even though the combined HERA-1 data set [25] itself has a small total uncertainty. Yet, the upcoming combination of HERA-1 heavy-quark cross sections is expected to improve constraints on m_c. The S-ACOT-χ implementation brings theoretical predictions up to matching accuracy by including the NNLO terms.

II. S-ACOT-χ SCHEME: THEORETICAL FRAMEWORK

Consider neutral-current DIS at energy that is sufficient to produce N_l light flavors (such as $l = u$, d and s) and one heavy flavor h ("charm") with mass m_h. The extension to production of several heavy flavors will be postponed until Sec. II D.

The GM scheme is designed so as to enable quick convergence of perturbative QCD series involving heavy quarks at any momentum transfer Q. Perturbative QCD cross sections in the GM scheme must converge reliably near the heavy-quark production threshold ($Q^2 \approx m_h^2$), as well as far above it ($Q^2 \gg m_h^2$), and smoothly interpolate between the limits. When Q is of order m_h, it is most natural to include all Feynman subgraphs with heavy-quark lines into the hard-scattering function (Wilson coefficient function). Such approach is called a "fixed-flavor number" (FFN) factorization scheme. $\mathcal{O}(\alpha_s^2)$ coefficient functions for massive quark DIS production in this scheme have been computed in [26–28]. At this Q, the NNLO coefficient functions in the GM scheme with $N_l + 1$ flavors are expected to reduce to the FFN massive cross sections in the FFN scheme with N_l flavors. On the other hand, at high virtualities ($Q^2 \gg m_h^2$), the NNLO GM cross sections should be indistinguishable from the

NNLO ZM cross sections [19–21]. In this limit, the heavy-quark contributions are dominated by asymptotic collinear contributions that are also fully known to $\mathcal{O}(\alpha_s^2)$ [12, 29–31]. Mellin moments for *some* structure functions and operator matrix elements [32–37] and dominant logarithmic contributions [38, 39] have been computed to $\mathcal{O}(\alpha_s^3)$.

A realization of such scheme called "ACOT" was developed in Refs. [2, 40] and proven for inclusive DIS to all orders in Ref. [3]. A non-zero PDF is assigned in this scheme to each quark flavor that can be produced in the final state at the given Q value. S-ACOT-χ is the most recent variant of the ACOT scheme that adds two beneficial features. First, coefficient functions derived from Feynman graphs with initial-state heavy quarks are simplified by neglecting non-critical m_c dependence [3, 4]. Second, threshold suppression is introduced by evaluating these coefficient functions as a function of $\chi \equiv x\left(1 + 4m_c^2/Q^2\right)$ instead of Bjorken x [5]. Both modifications follow from the factorization theorem for inclusive DIS [3] and produce predictions that are simpler, yet numerically accurate. They are included as a part of the NNLO implementation that is now presented.

A.   Overview of QCD factorization

A DIS structure function $F(x, Q)$, such as F_2 or F_L, is written in a factorized form as

$$F(x, Q) = \sum_{i=1}^{N_f^{fs}} e_i^2 \sum_{a=0}^{N_f} \int_x^1 \frac{d\xi}{\xi} \, C_{ia}\left(\frac{x}{\xi}, \frac{Q}{\mu}, \frac{m_h}{\mu}, \alpha_s(\mu)\right) \, \Phi_{a/p}(\xi, \mu)$$

$$\equiv \sum_{i=1}^{N_f^{fs}} e_i^2 \sum_{a=0}^{N_f} \left[C_{ia} \otimes \Phi_{a/p}\right](x, Q), \tag{1}$$

where $\Phi_{a/p}(\xi, \mu)$ is a parton distribution function (PDF) for a parton type a, light-cone momentum fraction ξ, and factorization scale μ. $C_{i,a}(\widehat{x}, Q/\mu, m_h/\mu, \alpha_s(\mu))$ are Wilson coefficient functions evaluated at $\widehat{x} = x/\xi$. Convolution integrals over ξ are indicated by "$\otimes$". Two sums appear on the right-hand side of Eq. (1), over all quark flavors $i = 1, ..., N_f^{fs}$ that couple to the virtual photon with fractional electric charges $e_i = 2/3$ or $-1/3$, and over parton flavors a in the PDF $\Phi_{a/p}$. The index a runs over quark flavors ($a = 1, ...N_f$ for $u, d, s, ...$) and the gluon ($a = 0$). Perturbative coefficients of neutral-current DIS are the same for quarks and antiquarks up to NNLO. For each combination of flavors i and a, summation of quark and antiquark contributions of these flavors is always implied, but not shown for brevity.

Eq. (1) distinguishes between N_f^{fs}, the number of quark flavors produced in the final state (fs), and N_f, the number of active quark flavors in α_s and PDFs. The distinction is important for the ensuing discussion, as generally N_f^{fs} is different from N_f [1]. N_f^{fs} is equal to the number of final-state flavors that can be produced at the given $\gamma^* p$ center-of-mass energy $W = Q\sqrt{1/x - 1}$. All produced quark states can couple to the photon, so that the outer summation in Eq. (1) runs up to $i = N_f^{fs}$.

On the other hand, N_f is a parameter of the renormalization and factorization schemes. It is commonly set equal to the number of quark flavors with the masses that are lighter than Q. Only flavors with $a \leq N_f$ have non-zero PDFs in the inner summation, but their actual number depends on the factorization scheme.

To determine $C_{i,a}$, we calculate auxiliary structure functions for scattering on an initial-state parton b, $F(e + b \to e + X) \equiv \sum_{i=1}^{N_f^{fs}} e_i^2 F_{i,b}$. The coefficient functions $C_{i,a}$ are infrared-safe parts of $F_{i,b}$. They enter convolutions together with parton-level PDFs $\Phi_{a/b}(\xi, \mu)$ for splittings $b \to a$, as

$$F_{i,b}(\widehat{x}, Q) = \sum_{a=1}^{N_f} \left[C_{i,a} \otimes \Phi_{a/b} \right] (\widehat{x}, Q). \tag{2}$$

In the $\overline{\text{MS}}$ scheme, the parton-level PDFs are given by matrix elements of bilocal field operators that can be computed in perturbation theory. For example, the PDF for finding a quark q in a massless parton b, in the light-like gauge, is

$$\Phi_{q/b}(\xi) = \int \frac{dy^-}{2\pi} e^{-\xi p^+ y^-} \langle b(p) | \overline{\psi}(0, y^-, \vec{0}_T) \gamma^+ \psi(0) | b(p) \rangle, \tag{3}$$

where the light-cone momentum components of the partons b and q are $p^\mu = \left\{ p^+, 0, \vec{0}_T \right\}$ and $k^\mu = \left\{ \xi p^+, m_q^2/(2\xi p^+), \vec{0}_T \right\}$, respectively, and $p^\pm \equiv (p^0 \pm p^3)/\sqrt{2}$.

The functions $F_{i,b}$, $C_{i,a}$, and $\Phi_{a/b}$ can be expanded as a series of $a_s \equiv \alpha_s(\mu, N_f)/(4\pi)$:

$$F_{i,b}(x) = F_{i,b}^{(0)}(x) + a_s F_{i,b}^{(1)}(x) + a_s^2 F_{i,b}^{(2)}(x) + \dots, \tag{4}$$

$$C_{i,a}(\widehat{x}) = C_{i,a}^{(0)}(\widehat{x}) + a_s C_{i,a}^{(1)}(\widehat{x}) + a_s^2 C_{i,a}^{(2)}(\widehat{x}) + \dots, \tag{5}$$

$$\Phi_{a/b}(\xi) = \delta_{ab}\delta(1 - \xi) + a_s A_{ab}^{(1)}(\xi) + a_s^2 A_{ab}^{(2)}(\xi) + \dots . \tag{6}$$

In the last equation, $A_{ab}^{(k)}$ ($k = 0, 1, 2, \dots$) are perturbative coefficients composed of DGLAP splitting functions $P_{ab}^{(k)}$, such as $A_{hg}^{(1)}(\xi) = 2\,P_{hg}^{(1)}(\xi)\,\ln\left(\mu^2/m_h^2\right)$ for the $g \to h\bar{h}$ splitting.

By equating coefficients on both sides of Eq. (2), order by order in a_s, we obtain

$$
\begin{aligned}
C_{i,b}^{(0)}(\widehat{x}) &= F_{i,b}^{(0)}(\widehat{x}), \\
C_{i,b}^{(1)}(\widehat{x}) &= F_{i,b}^{(1)}(\widehat{x}) - \left[C_{i,a}^{(0)} \otimes A_{ab}^{(1)} \right](\widehat{x}), \\
C_{i,b}^{(2)}(\widehat{x}) &= F_{i,b}^{(2)}(\widehat{x}) - \left[C_{i,a}^{(0)} \otimes A_{ab}^{(2)} \right](\widehat{x}) - \left[C_{i,a}^{(1)} \otimes A_{ab}^{(1)} \right](\widehat{x}).
\end{aligned}
\tag{7}
$$

Perturbative terms $C_{i,a}^{(k)}$ in the coefficient functions are thus derived from the perturbative expansions for $F_{i,b}$ and $\Phi_{a/b}$ upon implied summation over the repeating index a.

The coefficients $A_{ab}^{(k)}$ in $\Phi_{a/b}$ consist of large or singular terms arising in $F_{i,b}^{(k)}$ when the momenta of a and b are collinear. Subtraction of convolutions of the $A_{ab}^{(k)}$ terms from $F_{i,b}^{(k)}$ on the right-hand side of Eqs. (7) produces finite (infrared-safe) results for $C_{i,b}^{(k)}$.

Depending on the masses of a and b, two forms of $A_{ab}^{(k)}$ in these equations are possible. If both a and b are massless, $A_{ab}^{(k)}$ contains a singular part, given in $n = 4 - \epsilon$ dimensions by $\sum_{p=0}^{k}(1/\epsilon)^p s_{p,ab}$, where $s_{p,ab}$ contains a DGLAP splitting function; and a finite part (logs+finite terms) of the form $\sum_{p=0}^{k} \ln^p(\mu^2/\mu_{IR}^2)s'_{p,ab}$, where μ is the factorization scale, and μ_{IR} is the parameter of the dimensional regularization in the infrared limit.

When these "mass singularities" are subtracted as in Eqs. (7), one obtains infrared-safe parts $\widehat{F}_{i,b}^{(k)}$ of $F_{i,b}^{(k)}$, denoted by a caret:

$$
\widehat{F}_{i.b}^{(k)}\left(\widehat{x}, \frac{Q^2}{\mu^2}\right) = F_{i,b}^{(k)}\left(\widehat{x}, \frac{Q^2}{\mu_{IR}^2}, \frac{1}{\epsilon}\right) - \sum_{p=0}^{k} \left[C_{i,a}^{(p)} \otimes A_{ab}^{(k-p)} \right]\left(\widehat{x}, \frac{\mu^2}{\mu_{IR}^2}, \frac{1}{\epsilon}\right).
\tag{8}
$$

The difference $\widehat{F}_{i,b}^{(k)}$ is finite, even though both the "bare" functions $F_{i,b}^{(k)}$ and the PDF coefficients $A_{ab}^{(k)}$ contain the singular $1/\epsilon^p$ terms, where p is a positive integer.

If a massive parton a is produced from a massless parton b (as in $g \to c\bar{c}$ or $u \to g \to c\bar{c}$), the coefficients $A_{ab}^{(k)}$ consist solely of logarithms and finite terms involving mass m_a,

$$
A_{ab}^{(k)}\left(\xi, \frac{\mu^2}{m_a^2}\right) = \sum_{p=0}^{k} \ln^p(\mu^2/m_a^2)s'_{p,ab}(\xi).
\tag{9}
$$

The coefficient $A_{ab}^{(k)}$ is finite for $m_a \neq 0$, but $A_{ab}^{(k)} \to \infty$ when $\mu^2 \gg m_a^2$. For such massive quarks, the coefficients $A_{ab}^{(k)}$ appear as subtractions from the massive $F_{ib}^{(k)}$ in the expressions for $C_{i,a}^{(k)}$. In accordance with the S-ACOT scheme, the mass-dependent $A_{ab}^{(k)}$ only appear in explicit heavy-particle production, $i.e.$, when the transitions are of the type $b(m_b = 0) \to a(m_a \neq 0)$. All other subprocesses use massless expressions, constructed from renormalized parts $\widehat{F}_{i.b}^{(k)}\left(x, \frac{Q}{\mu}\right)$ given by Eq. (8).

B. Heavy-quark component F_h of inclusive $F(x,Q)$

To construct the Wilson coefficient functions explicitly, we decompose $F(x,Q)$ according to the (anti-)quark couplings to the photon [18]. Terms in which the photon couples to the light (l) or heavy (h) quark are designated as F_l and F_h, respectively:

$$F = \sum_{l=1}^{N_l} F_l + F_h, \tag{10}$$

with

$$F_l(x,Q) = e_l^2 \sum_a \left[C_{l,a} \otimes \Phi_{a/p} \right](x,Q), \tag{11}$$

and

$$F_h(x,Q) = e_h^2 \sum_a \left[C_{h,a} \otimes \Phi_{a/p} \right](x,Q). \tag{12}$$

Note that this separation is purely theoretical: F_l and F_h cannot be measured separately or distinguished in some other way. Furthermore, the heavy-quark component F_h is not the same as the semi-inclusive heavy-quark structure function $F_{h,SI}$ measured in experiments. The relation between $F_{h,SI}$ and F_h is clarified in Sec. II E, with the explicit formula given by Eq. (42).

Focusing first on the contribution F_h with the photon coupled to h, we obtain its Wilson coefficients $C_{h,a}(\widehat{x})$ from the parton-level functions $F_{h,b}$ via Eqs. (7):

$$
\begin{aligned}
&C_{h,a}^{(0)}(\widehat{x}) = \delta_{ha}\delta(1 - \widehat{x}); \\
&C_{h,g}^{(1)} = F_{h,g}^{(1)} - C_{h,h}^{(0)} \otimes A_{hg}^{(1)}; \quad C_{h,l}^{(1)} = C_{l,h}^{(1)} = 0; \quad C_{h,h}^{(1)} = F_{h,h}^{(1)} - C_{h,h}^{(0)} \otimes A_{hh}^{(1)}; \\
&C_{h,g}^{(2)} = F_{h,g}^{(2)} - C_{h,h}^{(0)} \otimes A_{hg}^{(2)} - C_{h,h}^{(1)} \otimes A_{hg}^{(1)} - C_{h,g}^{(1)} \otimes A_{gg}^{(1)}; \\
&C_{h,l}^{(2)} = F_{h,l}^{PS,(2)} - C_{h,h}^{(0)} \otimes A_{hl}^{PS,(2)} - C_{h,g}^{(1)} \otimes A_{gl}^{(1)}; \\
&C_{h,h}^{(2)} = F_{h,h}^{(2)} - C_{h,h}^{(0)} \otimes A_{hh}^{(2)} - C_{h,h}^{(1)} \otimes A_{hh}^{(1)} - C_{h,g}^{(1)} \otimes A_{gh}^{(1)}.
\end{aligned}
\tag{13}
$$

In these expressions, the coefficient $C_{h,l}^{(2)}$ with the initial-state light quark depends on flavor-non-diagonal, or pure-singlet (PS), components of $F_{i,j}^{(2)}$ and $A_{ij}^{(2)}$, defined by

$$G_{i,j} \equiv G_{i,j}^{PS} + \delta_{ij} G_{i,j}^{NS}, \text{ for } G_{i,j} = C_{i,j}^{(2)}, F_{i,j}^{(2)}, \text{ and } A_{i,j}^{(2)}. \tag{14}$$

On the other hand, the coefficient $C_{h,h}^{(2)}$ with the initial-state heavy quark depends both on the pure singlet (PS) and non-singlet (NS) components, as will be shown below.

Structure Functions

Subtractions

$c_{h,h}^{(0)}$ $F_{h,g}^{(1)}$

$c_{h,h}^{(1)}$

$F_{h,g}^{(2)}$ $F_{h,l}^{PS\,(2)}$

$c_{h,h}^{(2)}$

$A_{h,g}^{(1)} * c_{h,h}^{(0)}$

$A_{h,g}^{(1)} * c_{h,h}^{(1)}$

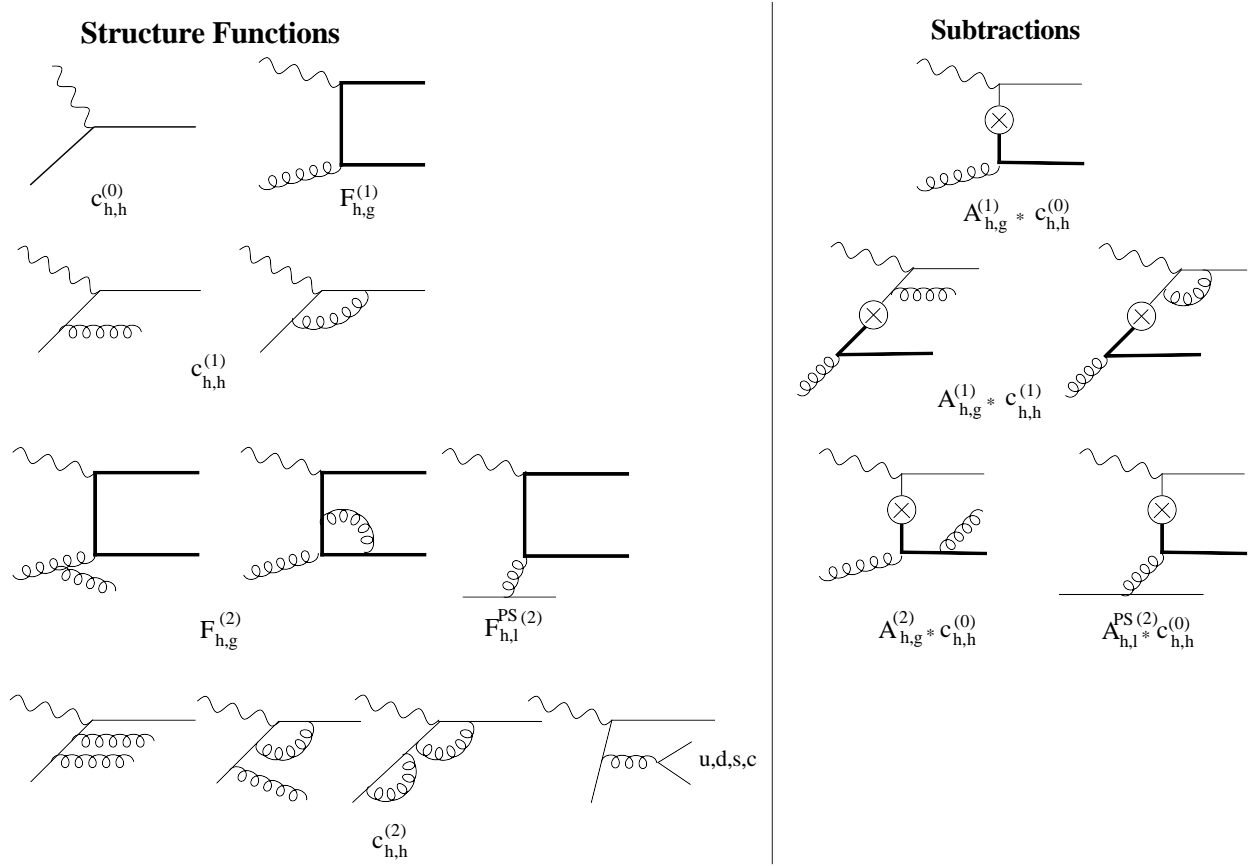$A_{h,g}^{(2)} * c_{h,h}^{(0)}$ $A_{h,l}^{PS\,(2)} * c_{h,h}^{(0)}$

FIG. 1: Representative scattering contributions to $F_h(x, Q)$.

Representative diagrams for heavy-quark contributions in Eqs. (13) are shown in Fig. 1. The reader may consult this figure frequently to identify various terms in the ensuing discussion. Propagators and external legs for quarks that are indicated by thick lines (thin lines) will eventually be computed with full mass dependence (in the massless approximation) .

The heavy-quark diagrams fall into two categories, those that do not involve a collinear approximation for scattering of heavy quarks (often called "flavor-creation", or FC, terms), and those that do (flavor-excitation, or FE, terms). While FC contributions must be evaluated exactly, the approximate nature of the FE terms allows some useful simplifications.

At $\mathcal{O}(\alpha_s^2)$, the flavor-creation contributions include the coefficients $F_{h,g}^{(1)}$, $F_{h,g}^{(2)}$, and $F_{h,l}^{PS,(2)}$. The heavy quarks appear in these terms inside the $O(\alpha_s)$ Feynman subgraph for $\gamma^* g \to h\bar{h}$, connected by a gluon propagator to an initial-state gluon or a light quark. These contributions are evaluated with the exact kinematical dependence on m_h, and hence are defined unambiguously.

The FE cross sections are proportional to the heavy-quark PDF that approximates

collinear production of heavy-quark pairs from light partons in the high-energy limit. Structure functions and coefficient functions with an initial-state heavy quark, such as $F_{h,h}^{(k)}$ and $C_{h,h}^{(k)}$, fall into this class. The FE coefficient functions reduce to unique $\overline{\text{MS}}$ expressions when m_h is negligible [3], but, near the threshold, they may differ by non-unique powerlike contributions $(m_h^2/Q^2)^p$ with $p > 0$. Within the ACOT scheme, several conventions have been proposed to include the powerlike contributions in a way compatible with the QCD factorization theorem.[2]

Among these conventions, the "full ACOT scheme" [2] evaluates the FE coefficient functions ($C_{h,h}^{(k)}$, etc.) with their complete mass dependence. The simplified ACOT (S-ACOT) scheme [3, 4] neglects *all* mass terms in $C_{h,h}^{(k)}$ and thereupon reduces tedious computations typical for the full ACOT scheme. The S-ACOT-χ scheme [5] adopted in our computation includes *the most important* mass dependence in $C_{h,h}^{(k)}$ and uses simpler zero-mass expressions everywhere else. It generalizes the slow-rescaling prescription for single heavy quark production in neutrino DIS at leading order [41] to other heavy final states and higher QCD orders.

If we use uppercase and lowercase letters to denote mass-dependent and massless quantities, and a caret to indicate renormalized ZM functions, the S-ACOT-χ convention for functions with initial-state heavy quarks can be summarized as

$$C_{h,h}^{(k)}\left(\frac{x}{\xi}, \frac{Q}{\mu}, \frac{m_h}{Q}\right) = c_{h,h}^{(k)}\left(\frac{\chi}{\xi}, \frac{Q}{\mu}, m_h = 0\right) \theta(\chi \leq \xi \leq 1), \tag{15}$$

and

$$F_{h,h}^{(k)}\left(\frac{x}{\xi}, \frac{Q}{\mu}, \frac{m_h}{Q}\right) = \widehat{f}_{h,h}^{(k)}\left(\frac{\chi}{\xi}, \frac{Q}{\mu}, m_h = 0\right) \theta(\chi \leq \xi \leq 1), \tag{16}$$

where

$$\chi = x\left(1 + \frac{(\sum_{fs} m_h)^2}{Q^2}\right), \tag{17}$$

and $\sum_{fs} m_h$ is the net mass of all heavy particles produced in the final state. With the exception of a few very rare subprocesses identified below, at most one heavy-quark pair is produced in all cases that we consider. Without losing accuracy, we therefore assume $\chi = x\left(1 + \frac{4m_h^2}{Q^2}\right)$ throughout the computation.

---

[2] The differences between these conventions are formally of a higher order in α_s, but some conventions lead to faster perturbative convergence.

This form is motivated by an observation that the largest powerlike terms are associated with the constraint imposed on the convolution by energy conservation in production of heavy final states [42]. The ZM functions here depend on the variable χ instead of Bjorken x as an input parameter, and the momentum fraction in their convolutions is integrated over the range $\chi \leq \xi \leq 1$. The χ convention is justified in the context of the QCD factorization theorem in Sec. II F. Its numerical impact is discussed in Sec. III D.

When the S-ACOT-χ scheme is adopted, Eqs. (13) become

$$c_{h,a}^{(0)} = \delta_{ha}\delta(1 - \widehat{\chi}); \quad c_{h,h}^{(1)} = \widehat{f}_{h,h}^{(1)}; \tag{18}$$

$$C_{h,g}^{(1)} = F_{h,g}^{(1)} - A_{hg}^{(1)}; \tag{19}$$

$$C_{h,g}^{(2)} = \widehat{F}_{h,g}^{(2)} - A_{hg}^{(2)} - c_{h,h}^{(1)} \otimes A_{hg}^{(1)}; \tag{20}$$

$$c_{h,h}^{(2)} = \widehat{f}_{h,h}^{(2)}; \quad C_{h,l}^{(2)} = \widehat{F}_{h,l}^{PS,(2)} - A_{hl}^{PS,(2)}. \tag{21}$$

Lowercase functions on the right-hand side of these equations are given by ZM expressions. Among all terms, only the structure functions $F_{h,g}^{(1)}$, $\widehat{F}_{h,g}^{(2)}$, and $\widehat{F}_{h,l}^{PS,(2)}$ are calculated with the exact mass dependence. The carets above $\widehat{F}_{h,g}^{(2)}$ and $\widehat{F}_{h,l}^{PS,(2)}$ indicate that the massless $1/\epsilon$ pole terms, $C_{h,g}^{(1)} \otimes A_{gg}^{(1)}$ and $C_{h,g}^{(1)} \otimes A_{gl}^{(1)}$, have been subtracted from them.

In the rest of the terms, the input longitudinal variable is set to be $\widehat{\chi} = \chi/\xi$. The convolution of such term $f(\widehat{\chi})$ with the PDF $\Phi(\xi)$ is

$$[f \otimes \Phi](\zeta) \equiv \int_\zeta^1 \frac{d\xi}{\xi} f\left(\frac{\zeta}{\xi}\right) \Phi(\xi), \tag{22}$$

where $\zeta = \chi$. [The naive massless approximation is $\zeta = x$.]

The one-loop expressions $\widehat{f}_{h,h}^{(k)}$, $F_{h,g}^{(1)}$, and $A_{h,g}^{(1)}$ can be found in [2, 12, 43]. $\widehat{F}_{h,g}^{(2)}$ and $\widehat{F}_{h,l}^{PS,(2)}$ coincide with the massive structure functions with initial-state gluons and pure-singlet light quarks in [26, 27]. They are independent of N_l. The expressions for $A_{hg}^{(2)}$ and $A_{hl}^{(2)}$ are computed as $A_{Hg}^{(2)}$ and $A_{Hq}^{(2)}$ in [12].

The $\mathcal{O}(\alpha_s^2)$ contribution $c_{h,h}^{(2)} = \widehat{f}_{h,h}^{(2)}$ corresponds to radiation of up to $N_l + 1$ flavors of $q\bar{q}$ pairs off an incoming quark h. It can be found as a sum of the pure-singlet and non-singlet ZM coefficient functions from Refs. [19–21, 44, 45]:

$$c_{h,h}^{(2)} = c_{h,h}^{PS,(2)} + c_{h,h}^{NS,(2)} = \widehat{f}_{h,h}^{(2)} = \widehat{f}_{h,h}^{PS,(2)} + \widehat{f}_{h,h}^{NS,(2)}. \tag{23}$$

In this equation, both pure-singlet and non-singlet parts of $\widehat{f}_{h,h}^{(2)}$ are taken to be massless, which is one of the choices possible within the S-ACOT scheme. Note that the $c_{h,h}^{(2)}$ functions
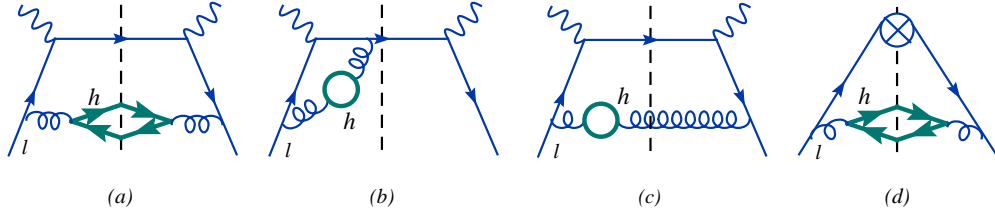
FIG. 2: Disconnected heavy-quark contributions to $F_{l,l}^{NS,(2)}$ (a,b,c) and $A_{l,l}^{NS,(2)}$ (d).

with three indicated final-state h (anti-)quarks and an unobserved fourth h (anti-)quark among the target remnants could justifiably use a more restrictive rescaling variable, $\chi = x\left(1 + \frac{16m_h^2}{Q^2}\right)$, as their parameter. Since their respective contributions are vanishingly small, it suffices to evaluate them with the same variable $\chi = x\left(1 + \frac{4m_h^2}{Q^2}\right)$ as in the rest of the terms to simplify the implementation.

It is equally acceptable to evaluate the pure-singlet $F_{h,h}^{PS,(2)}$ with a massive $\gamma^* g \to h\bar{h}$ subgraph, so that the corresponding coefficient function is given by the massive $C_{h,l}^{(2)}$ in Eq. (21). In this case, $F_{h,h}^{PS,(2)}$ can be combined with the pure-singlet contribution with initial-state light quarks, also given by $C_{h,l}^{(2)}$. The complete $\mathcal{O}(\alpha_s^2)$ part of $F_h(x, Q)$ then takes a simple form

$$F_h^{(2)} = e_h^2 \left\{ c_{h,h}^{NS,(2)} \otimes (\Phi_{h/p} + \Phi_{\bar{h}/p}) + C_{h,l}^{(2)} \otimes \Sigma + C_{h,g}^{(2)} \otimes \Phi_{g/p} \right\}, \tag{24}$$

where $\Sigma(x, \mu)$ is the singlet quark PDF summed over $N_f = N_l + 1$ flavors:

$$\Sigma(x, \mu) = \sum_{i=1}^{N_f} \left[\Phi_{i/p}(x, \mu) + \Phi_{\bar{i}/p}(x, \mu) \right]. \tag{25}$$

We use Eq. (24) for practical implementation of F_h, with the coefficient functions computed as in Eqs. (20) and (21).

C. Light-quark component of $F(x,Q)$

By a similar argument, Eq. (7) serves as a starting point for finding coefficient functions for the light-quark component $F_l(x,Q)$. The corresponding Wilson coefficients are

$$c_{l,a}^{(0)} = \delta_{la}\delta(1-x);$$

$$C_{l,l}^{(1)} = F_{l,l}^{(1)} - C_{l,l}^{(0)} \otimes A_{ll}^{(1)}; \quad C_{l,g}^{(1)} = F_{l,g}^{(1)} - C_{l,l}^{(0)} \otimes A_{lg}^{(1)}; \quad C_{l,h}^{(1)} = C_{l,l'}^{(1)} = 0;$$

$$C_{l,l}^{(2)} = F_{l,l}^{PS,(2)} + F_{l,l}^{NS,(2)} - C_{l,l}^{(0)} \otimes \left[A_{ll}^{PS,(2)} + A_{ll}^{NS,(2)}\right] - C_{l,l}^{(1)} \otimes A_{ll}^{(1)} - C_{l,g}^{(1)} \otimes A_{gl}^{(1)};$$

$$C_{l,l'}^{(2)} = F_{l,l'}^{PS,(2)} - C_{l,l}^{(0)} \otimes A_{ll'}^{PS,(2)} - C_{l,g}^{(1)} \otimes A_{gl'}^{(1)};$$

$$C_{l,h}^{(2)} = F_{l,h}^{PS,(2)} - C_{l,l}^{(0)} \otimes A_{lh}^{PS,(2)} - C_{l,g}^{(1)} \otimes A_{gh}^{(1)};$$

$$C_{l,g}^{(2)} = F_{l,g}^{(2)} - C_{l,l}^{(0)} \otimes A_{lg}^{(2)} - C_{l,l}^{(1)} \otimes A_{lg}^{(1)} - C_{l,g}^{(1)} \otimes A_{gg}^{(1)}. \tag{26}$$

The quark-to-quark Wilson coefficients $C_{l,l}^{(2)}$, $C_{l,h}$, and $C_{l,l'}^{(2)}$ (for $l' \neq l$) are decomposed into their PS and NS components as in Eq. (14). Non-singlet contributions $F_{l,l}^{NS,(2)}$ and $A_{ll}^{NS,(2)}$ contain squared matrix elements with heavy-quark lines that are disconnected from the initial-state proton, as in Fig. 2. These diagrams must be evaluated with full dependence on m_h. The rest of the coefficients in Eqs. (26) do not contain disconnected heavy-quark lines. They are computed according to ZM formulas.

Explicitly, the non-singlet functions with mass dependence consist of two parts, arising either from Feynman diagrams with light partons only (designated as g_{light}), or with a heavy quark in the final-state emission or virtual loop (denoted by $G_{heavy}(m_h)$):

$$G = g_{light} + G_{heavy}(m_h),$$

where $G = F_{l,l}^{NS,(2)}$ or $A_{l,l}^{NS,(2)}$. The function $G_{heavy}(m_h)$, provided by the graphs of the type shown in Fig. 2, retains complete m_h dependence. The function g_{light}, obtained from the same graphs as in Fig. 2, but with the heavy quark h replaced by one of the light quarks $(u,d,...)$, is evaluated in the ZM approximation.

Masses can be neglected in the rest of Eqs. (26), so we get

$$c_{l,a}^{(0)} = \delta_{la}\delta(1-x); \tag{27}$$

$$c_{l,l}^{(1)} = \widehat{f}_{l,l}^{(1)}; \quad c_{l,g}^{(1)} = \widehat{f}_{l,g}^{(1)}; \quad c_{l,h}^{(1)} = c_{l,l'}^{(1)} = 0; \tag{28}$$

$$C_{l,l}^{(2)} = C_{l,l}^{NS,(2)} + c^{PS,(2)}, \text{ where} \tag{29}$$

$$C_{l,l}^{(2),NS} = \widehat{f}_{l,l,light}^{NS,(2)} + F_{l,l,heavy}^{NS,(2)} - A_{ll,heavy}^{NS,(2)}; \tag{30}$$

$$c_{l,h}^{(2)} = c_{l,l'}^{(2)} = c^{PS,(2)}; \quad c_{l,g}^{(2)} = \widehat{f}_{l,g}^{(2)}. \tag{31}$$

The 1-loop coefficients $c_{l,a}^{(1)}$ have been known for a long time [46–48]. The 2-loop massless contributions in Eqs. (30) and (31) can be derived from the published ZM results according to the following procedure. Using the decomposition Eq. (14) for $c_{i,j}$ in the ZM scheme,

$$c_{i,j} \equiv c^{PS} + \delta_{ij} c^{NS,(2)}, \tag{32}$$

where c^{PS} and c^{NS} are independent of the quark flavors i or j given that the masses are neglected, we write

$$F(x, Q) = \sum_{i,a} e_i^2 \left[c_{i,a} \otimes \Phi_{a/p} \right] = \sum_i e_i^2 \left\{ \sum_j \left(c^{PS} + \delta_{ij} c^{NS} \right) \otimes \Phi_{j/p} + c_g \otimes \Phi_{g/p} \right\}$$
$$= \left[c^{NS} \otimes \Sigma^{+,NS} \right] + \frac{\left(\sum_i e_i^2 \right)}{N_f} \left\{ \left[c^S \otimes \Sigma \right] + N_f \left[c_g \otimes \Phi_{g/p} \right] \right\}, \tag{33}$$

with

$$c^S \equiv c^{NS} + N_f c^{PS}.$$

The singlet PDF $\Sigma(x, \mu)$ is given by Eq. (25), and the non-singlet sum of (anti-)quark PDFs is

$$\Sigma^{+,NS}(x, \mu) = \sum_{i=1}^{N_f} e_i^2 \left(\Phi_{i/p}(x, \mu) + \Phi_{\bar{i}/p}(x, \mu) - \frac{1}{N_f} \Sigma(x, \mu) \right).$$

Eq. (33) expresses $F(x, Q)$ in the same representation as Eq. (4.1) in the N³LO calculation of DIS cross sections [45]. Comparing Eqs. (30) and (31) with ZM coefficient functions in Section 4 of that reference (which are indicated here by an asterisk " $*$ "), we find that

$$c^{PS,(2)} = c_{I,ps}^{(2,*)}/N_f, \tag{34}$$

$$\widehat{f}_{i,g}^{(2)} = c_{I,g}^{(2,*)}/N_f, \tag{35}$$

and

$$\widehat{f}_{l,l,light}^{NS,(2)} = c_{I,ns}^{(2,*)}(n_f = N_l), \tag{36}$$

with $I = 2$ or L for $F_2(x, Q)$ and $F_L(x, Q)$, respectively.

The non-singlet heavy-quark coefficient function,

$$F_{l,l,heavy}^{NS,(2)}(x, Q^2/m_h^2) = \left(L_{I,q}^{NS,(2)}(x, Q^2/m_h^2) \right)_+ + \frac{2}{3} \ln \left(\frac{Q^2}{m_h^2} \right) c_{l,l}^{(1)}(x), \tag{37}$$

is composed of contributions of several classes shown in Figs. 2(a)-(c). Diagrams with real emission of a heavy-quark pair (as in Fig. 2(a)) in $F_I(x, Q)$ contribute a function $L_{I,q}^{NS,(2)}(x, Q^2/m_h^2)$ in Eqs. (A.1) and (A.2) of Ref. [49]. This contribution is combined with

the virtual two-loop diagrams, cf. Fig. 2(b), to produce the first term on the right-hand side of Eq. (37), in which $L_{I,q}^{NS,(2)}(x, Q^2/m_h^2)$ is regularized by the plus prescription at $x \to 1$. Contributions with a heavy-quark polarization graph inserted into a one-loop $\gamma^* q$ scattering diagram, of the kind shown in Fig. 2(c), produce the second term in Eq. (37), where $c_{l,l}^{(1)}$ is available from Refs. [46–48].

In this derivation, we do not explicitly compute the virtual loop contribution in Fig. 2(b), but deduce it from the Adler sum rule [50–53]. The sum rule states that the sum of the real and virtual contributions to $F_{l,l,heavy}^{NS,(2)}(x, Q^2/m_h^2)$ satisfies

$$\int_0^1 F_{l,l,heavy}^{NS,(2)}(x, Q^2/m_h^2)\, dx = 0. \tag{38}$$

With this rule, it can be demonstrated that the virtual contribution amounts to imposing the plus prescription on $L_{I,q}^{NS,(2)}(x, Q^2/m_h^2)$ as in Eq. (37).

In the asymptotic limit $Q^2 \gg m_h^2$, $F_{l,l,heavy}^{NS,(2)}$ for the inclusive F_2 contains large terms proportional to $\ln(Q^2/m_h^2)$. Those coincide with the $\mathcal{O}(\alpha_s^2)$ non-singlet part $A_{l,l,heavy}^{NS,(2)}$ of the light-quark PDF that includes radiation of a heavy-quark pair as shown in Fig. 2(d). $A_{l,l,heavy}^{NS,(2)}$ is computed as $A_{qq,H}^{NS,(2)}(z, m_h^2/\mu^2)$ in Eq. (B.4) of Ref. [12], which we evaluate as a function of $z = \chi/\xi$ in accord with the S-ACOT-χ scheme.

When $A_{l,l,heavy}^{NS,(2)}$ is subtracted from $F_{l,l,heavy}^{NS,(2)}$ as in Eq. (30), the difference is free of the collinear logs. After the difference is combined with the light-quark-only contributions $\widehat{f}_{l,l,light}^{NS,(2)}$, we obtain the full non-singlet coefficient function $C_{l,l}^{(2),NS}$, which coincides in the limit $m_h^2/Q^2 \to 0$ with its zero-mass $\overline{\text{MS}}$ expression in Eq. (8) of Ref. [20]. For the longitudinal function F_L, the heavy-quark subtraction $A_{l,l,heavy}^{NS,(2)}$ is zero. Putting everything together, we obtain the final expression for the NNLO light-quark component,

$$F_l^{(2)} = e_l^2 \left\{ C_{l,l}^{NS,(2)} \otimes (\Phi_{l/p} + \Phi_{\bar{l}/p}) + c^{PS,(2)} \otimes \Sigma + c_{l,g}^{(2)} \otimes \Phi_{g/p} \right\}, \tag{39}$$

where the Wilson coefficients are listed in Eqs. (29)-(31) and (34)-(37).

D. Several heavy flavors

The structure functions F_l and F_h in Eqs. (39) and (24) are all that is needed to compute inclusive $F(x, Q)$. Our expressions can be readily extended to include two or more heavy-
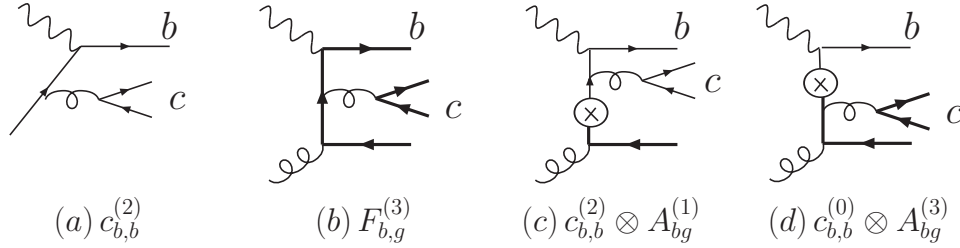
FIG. 3: Examples of α_s^2 and α_s^3 contributions with heavy-quark lines of different flavors.

quark flavors:

$$F = \sum_{l=1}^{N_l} F_l + \sum_{h=N_{l+1}}^{N_f^{fs}} F_h, \tag{40}$$

where the sum runs over all quark flavors satisfying $4m_h^2 \leq W^2$ (*i.e.*, up to the number N_f^{fs} of the kinematically allowed final-state flavors).

Beginning at $\mathcal{O}(\alpha_s^2)$, some contributions to F_h include heavy quarks of two different flavors, say, c and b. For instance, Fig. 3(a) shows a two-loop diagram in F_b in which an incoming bottom quark radiates a $c\bar{c}$ pair before or after the scattering on the photon. This flavor-excitation contribution, relevant at Q large enough, is evaluated by a massless expression, $c_{b,b}^{(2)}(m_c = m_b = 0) \otimes \Phi_{b/p}(\chi, \mu)$, in accord with the main rule of the S-ACOT scheme. We take the rescaling variable to be $\chi = x\,(1 + 4m_b^2/Q^2))$, given the numerical smallness of the cross section, even though a more restrictive choice $\chi = x\,(1 + (2\,m_b + 2\,m_c)^2/Q^2))$ conforms better with the exact momentum conservation in production of a $b\bar{b} + c\bar{c}$ pair.

The above contribution resums the large-Q logarithmic behavior of a three-loop function $F_{b,g}^{(3)}$ for the process $\gamma^* g \to b\bar{b}c\bar{c}$. A representative Feynman diagram is shown in Fig. 3(b), with the rest of the diagrams in the class related to the shown diagram by re-attaching the $g \to c\bar{c}$ branch to one of the external legs (g, b, or $\bar{b}$).

In the $Q^2 \to \infty$ limit, $F_{b,g}^{(3)}$ *simultaneously* contains logarithms $\ln(Q^2/m_c^2)$ and $\ln(Q^2/m_b^2)$ that must be subtracted in order to obtain an infrared-safe coefficient function $C_{b,g}^{(3)}$. The subtraction is realized by applying the perturbative expansion procedure discussed in Section II B to the three-loop level. We get

$$C_{b,g}^{(3)} = F_{b,g}^{(3)} - c_{b,b}^{(2)} \otimes A_{bg}^{(1)} - c_{b,b}^{(0)} \otimes A_{bg}^{(3)}, \tag{41}$$

where the last two terms on the right-hand side are the subtractions associated with the diagrams of the type shown in Figs. 3(c) and (d). The functions $F_{b,g}^{(3)}$, $A_{bg}^{(1)}$, and $A_{bg}^{(3)}$ are

evaluated with full dependence on m_c and m_b. [The coefficient $A_{bg}^{(3)}$ has been recently computed in Ref. [37].] The coefficient functions $c_{b,b}^{(0)}$ and $c_{b,b}^{(2)}$ are massless.

Based on the general structure of the S-ACOT scheme, we expect the first and third term in Fig. 3 to cancel when $Q^2 \approx m_b^2$, and the fourth term to cancel the $\mathcal{O}(\alpha_s^3)$ contribution to the $c_{b,b}^{(0)} \otimes \Phi_{b/p}$ term in the same limit. The third and fourth terms cancel the $\ln(Q^2/m_c^2)$ and $\ln(Q^2/m_b^2)$ contributions to the second term, $F_{b,g}^{(3)}$, in the limit $Q^2 \gg m_b^2$. The numerical realization of these cancellations at three loops is still in the future, pending on the calculation of the unknown massive three-loop coefficients. The factorization theorem is indicative of the structure of the S-ACOT-χ subtraction terms that will arise at that order.

E.   Semi-inclusive heavy quark production

A clarification is needed that the heavy-quark component F_h of inclusive $F(x, Q)$ (defined as the part proportional to the heavy-quark electric charge e_h^2) is not directly measurable. Rather, experiments publish the semi-inclusive (SI) heavy-quark structure function $F_{h,SI}(x, Q)$ that is determined from the cross section with at least one registered heavy meson. In the case of F_2 at NNLO, $F_{h,SI}(x, Q)$ with $h = c$ essentially coincides with the charm structure function $F_2^{(c)}$ that is commonly measured by HERA experiments.

While $F_{h,SI}$ must be defined with care to obtain infrared-safe results at all Q [13], for a global fit it is sufficient to approximate $F_{h,SI}$ in the following way [18]. At moderate Q values accessible at HERA, we define it as

$$F_{h,SI}(x, Q) = F_h(x, Q) + \sum_{l=1}^{N_l} e_l^2 L_{I,q}^{NS,(2)} \otimes (\Phi_{l/p} + \Phi_{\bar{l}/p}). \tag{42}$$

Here $F_h(x, Q)$ is the component with the heavy quark struck by the photon, cf. Eqs. (12) and (24). $L_{I,q}^{NS,(2)}$ is the non-singlet part of the light-quark component $F_l(x, Q)$ that contains radiation of a $h\bar{h}$ pair in the final state, as shown in Fig. 2(a). This is the same function that was discussed in the previous subsection and computed expressly in Ref. [49]. However, since the virtual diagram in Fig. 2(b) does not contribute to $F_{h,SI}$, the plus prescription is not imposed on $L_{I,q}^{NS,(2)}$ in this case.

The $F_{h,SI}(x, Q)$ function that is thus defined is numerically stable in comparisons to the existing data [18]. Our numerical analysis shows that the contribution associated with

$L^{NS,(2)}_{I,q}$ provides between 0 and 3% of the semi-inclusive charm cross sections at $Q < 10$ GeV, which is insignificant compared to typical experimental errors.

F.   Factorization and χ convention

In the remainder of this section, we show that the S-ACOT-χ scheme is fully compatible with the QCD factorization theorem for DIS.

To see why the χ convention is needed, consider again the heavy-quark contribution to $F(x, Q)$ on the proton from Eq. (12),

$$F_h(x, Q) = e_h^2 \sum_{l=1}^{N_l} \int_\chi^1 \frac{d\xi}{\xi} C_{h,l} \left(\xi p, m_h, \frac{Q}{\mu_0} \right) \Phi_{l/p}(\xi, \mu_0). \tag{43}$$

This expression is for the same Q value as in Eq. (12), but the factorization scale $\mu_0 \approx 1$ GeV is taken to be below the switching-point scale for $N_l + 1$ flavors, so that only PDFs for light parton flavors ($l = 0, ... N_l$) are present. For this scale choice, the PDFs $\Phi_{l/p}(\xi, \mu_0)$ do not include subgraphs with the heavy-quark lines: those are contained solely in the Wilson coefficient functions $C_{h,l} \left(\xi p, m_h, \frac{Q}{\mu_0} \right)$. The right-hand side is non-zero when the light parton l carries enough energy to produce at least one $h\bar{h}$ pair in the final state. This condition is reflected in the integration limits $\chi \leq \xi \leq 1$ that are imposed on the convolution by the energy conservation constraints inside the coefficient functions $C_{h,l}$.

If μ is gradually increased above μ_0, a coefficient function $C_{h,h}$ with an initial-state heavy quark is introduced when μ crosses the switching point from N_l to $N_l + 1$ active flavors. This function does not automatically vanish outside of the physical range $\chi \leq \xi \leq 1$. If $C_{h,h}$ is defined so as to contribute in a wider range $\xi_{min} \leq \xi \leq 1$ at the switching point, with $x \leq \xi_{min} < \chi$, then the DGLAP evolution preserves the same wider range at all μ above the switching point.

If $\widehat{W}$ is the center-of-mass energy of the photon scattering on a *light* parton a,

$$\widehat{W}^2 \equiv (p_a + q)^2 = Q^2 \left(\xi/x - 1 \right), \tag{44}$$

a final state with several heavy particles of the net mass $\sum m_h$ is produced when

$$\left(\sum m_h \right)^2 \leq \widehat{W}^2 \leq W^2 = Q^2(1/x - 1). \tag{45}$$

According to this condition, the momentum fraction ξ must be in the range

$$\chi \leq \xi \leq 1, \tag{46}$$

for production to occur, where $\chi = x \left(1 + (\sum m_h)^2/Q^2\right) \geq x$.

If collinear approximations for flavor-excitation (FE) and subtraction terms in $C_{h,a}$ violate this fundamental requirement, large spurious contributions from the unphysical kinematical region cancel to each order of α_s, but survive as higher-order logarithmic terms. They can be eliminated by a supplemental condition that the correct integration limits are always to be preserved, as in Eq. (46).[3]

We will now show how to apply this condition at any order by including it into the QCD factorization theorem. For this purpose, we examine the projection operator Z that encapsulates the main rules of each factorization scheme [3]. It applies a set of approximations to the Feynman graphs with leading momentum regions in order to enable all-order factorization.

We will closely follow the derivation and notations in Ref. [3]. In this approach, the Feynman graphs containing the leading DIS contributions are composed of two-particle irreducible subgraphs H and T, joined by one parton line on each side of the unitarity cut. Each leading graph $H \cdot T$ involves integration over the momentum k^μ of the intermediate parton and summation over its spin components,

$$H \cdot T \equiv \sum_{a=g,u,\bar{u},d,\bar{d},...} \int \frac{d^4k}{(2\pi)^4} \sum_{spins} H_a(q,k) T_a(k,p). \tag{47}$$

Virtualities of all momenta are of order Q in the hard subgraph $H_a(q,k)$, and they are much smaller than Q in the target subgraph $T_a(k,p)$. H eventually contributes to the Wilson coefficient functions, and T to the PDFs. q^μ and p^μ are the photon's and proton's 4-momenta. The nearly massless proton moves in the $+z$ direction in the Breit reference frame.

The purpose of the Z operator is to approximate the leading-power (logarithmically

---

[3] Even in the $Q^2 \gg m_h^2$ limit, convolutions with FE terms and subtractions could be in principle extended to include contributions from $0 \leq \xi \leq x$. This would not violate QCD factorization order by order, but will destabilize higher-order terms. This is avoided by an implicit assumption that the FE convolutions in the ZM limit are restricted to the physical range $x \leq \xi \leq 1$.

divergent) part of $H \cdot T$ by a simpler expression, denoted by $H \cdot Z \cdot T$, and to recast $H \cdot T$ as

$$H \cdot T = \sum_a \int \frac{d^4k}{(2\pi)^4} \int \frac{d^4l}{(2\pi)^4} \sum_{spins} H_a(q,l) \, Z_a(l,k;\widehat{l}) \, T_a(k,p) + \text{non-leading power term.}$$

(48)

The leading-power approximation $H \cdot Z \cdot T$ provides the bulk of $H \cdot T$. The non-leading power part is suppressed by terms of order

$$\left(\frac{\text{highest virtuality in } T}{\text{lowest virtuality in } H} \right)^r, \text{ with } r > 0.$$

When it is recursively applied to all leading subgraphs, the Z projection generates the factorized expression for the structure function, $F = \sum_a [C_a \otimes f_a] + \mathcal{O}(\Lambda_{QCD}/Q)$. [3]

The Z operation simplifies integration over the momentum and summation over the spin components of the intermediate parton, and it also simplifies the hard graph H. The momentum l^μ of the parton a that enters H is replaced by a simpler momentum $\widehat{l}^\mu$, e.g., $\widehat{l}^\mu = \xi p^\mu$ if a is massless (where $0 \le \xi \le 1$). The Z operation discards power-suppressed terms in H, such as the masses of the light quarks that are always negligible compared to Q. It also specifies when the heavy-quark mass terms are to be retained in H, depending on the type of the factorization scheme and the partonic scattering subprocess.

In all variants of the ACOT scheme, the Z operator is the same in all partonic channels except for the H subgraphs with an incoming heavy-quark line. The target parts T_a, operators Z_l and Z_g for the H subgraphs with initial light-quark and gluon lines are identical in all variants, while the operator Z_h for the H subgraphs with incoming heavy quarks is not. The PDFs in T_a are defined by the operator matrix elements as in Eq. (3) and retain dependence on quark masses of all contributing flavors.

The Z_h operator is of the form

$$Z_h(l,k;\widehat{l}) = \frac{1}{4} (2\pi)^4 \, S_H(\widehat{l}) \, S_T \, \delta(l^+ - \widehat{l}^+) \delta(l^- - \widehat{l}^-) \delta^2(\vec{l}_T),$$

where $S_H(\widehat{l})$ and $S_T = \gamma^+$ are projectors on the leading spin components in H and T, respectively. The incoming heavy quark in H_h has an approximate momentum $\widehat{l}^\mu$, where the light-cone components of $\widehat{l}^\mu$ in the Breit frame are $\widehat{l}^\pm \equiv \left(\widehat{l}^0 \pm \widehat{l}^3 \right)/\sqrt{2}$ and $\vec{l}_T = 0$. With this representation, the $H_h \cdot Z_h \cdot T_h$ integral assumes the form of a convolution over ξ,

$$H_h \cdot Z_h \cdot T_h = \int \frac{d\xi}{\xi} \text{tr} \left[H_h(q,\widehat{l}) \frac{S_H(\widehat{l})}{2} \right] \int \frac{dk^- d^2\vec{k}_T}{(2\pi)^4} \text{tr} \left[\frac{\gamma^+}{2} T_h(k,p) \right],$$

(49)

Scheme	$\widehat{l}^{\mu}$ in Z_h	S_H	m_h in $H_h(q,\widehat{l})$	ξ range in $H_h \cdot T_h$
ACOT	$\left(\xi p^+, \frac{m_h^2}{2\xi p^+}, \vec{0}_T\right)$	$\frac{\widehat{l}\cdot\gamma+m_h}{\xi p^+}$	$m_h \neq 0$	$\frac{x}{2}\left(1+\sqrt{1+\frac{4m_h^2}{Q^2}}\right) \leq \xi \leq 1$
S-ACOT	$\left(\xi p^+, 0, \vec{0}_T\right)$	γ^-	$m_h = 0$	$x \leq \xi \leq 1$
S-ACOT-χ	$\left(\xi \frac{p^+}{1+4m^2/Q^2}, 0, \vec{0}_T\right)$	γ^-	$m_h = 0$	$x\left(1+4m_h^2/Q^2\right) \leq \xi \leq 1$

TABLE I: Components of the projection operator $Z_h(l,k;\widehat{l})$ in three versions of the ACOT scheme.

where $\xi = \widehat{l}^+/p^+$ is the ratio of the large "+" momentum components.

Table I collects expressions for $\widehat{l}^{\mu}$ and $S_H(\widehat{l})$ in the ACOT, S-ACOT, and S-ACOT-χ schemes. It also lists the integration ranges in the $H_h \cdot T_h$ convolutions and indicates if m_h is set to zero in the H_h subgraphs. We re-emphasize that the three schemes listed in the table are distinguished only by the hard subgraphs, or Wilson coefficients, with initial-state heavy quarks, i.e., in the flavor-excitation channel. The differences arise solely in the terms proportional to powers of m_h^2/Q^2 in $H_h(q,l)$. One could simplify the FE hard-scattering contributions by setting $m_h = 0$ as in the S-ACOT scheme. In the full ACOT scheme, the lower limit of integration in $H_h \cdot Z_h \cdot T_h$ is set by the kinematics of scattering of a massive quark into a massive quark, which violates the momentum conservation condition of Eq. (43) for pair production of massive quarks from light-quark scattering. In the S-ACOT scheme, one is tempted to set the integration range to $x \leq \xi \leq 1$, which is also incompatible with momentum conservation. One cannot just restrict the integration range to $\chi \leq \xi \leq 1$, as this disallows the lowest-order FE contribution $c_{h,h}^{(0)} \otimes h$ that contributes at $\xi = x$.

A better way is provided by the rescaling $\xi \to \widetilde{\xi} = \kappa\xi$, $p^+ \to \widetilde{p}^+ = p^+/\kappa$, which leaves $H(q,\widehat{l})$ invariant, as it does not change $\widehat{l}^{\mu}$, $\widehat{x} = Q^2/(2\widehat{l}\cdot q)$, or other kinematical variables in $H(q,\widehat{l})$. At the same time, rescaling changes the integration range for ξ in the convolution.

Choosing $\kappa = 1 + (\sum m_h)^2/Q^2$, we obtain the S-ACOT-$\chi$ scheme that has all desirable features:

1. The proof of QCD factorization for the S-ACOT scheme in [3] also applies to the S-ACOT-χ scheme, since the S-ACOT and S-ACOT-χ schemes have the same $H(q,\widehat{l})$. The Z operation of the S-ACOT-χ scheme upholds all expected properties that are listed in Sec. 9C of [3].
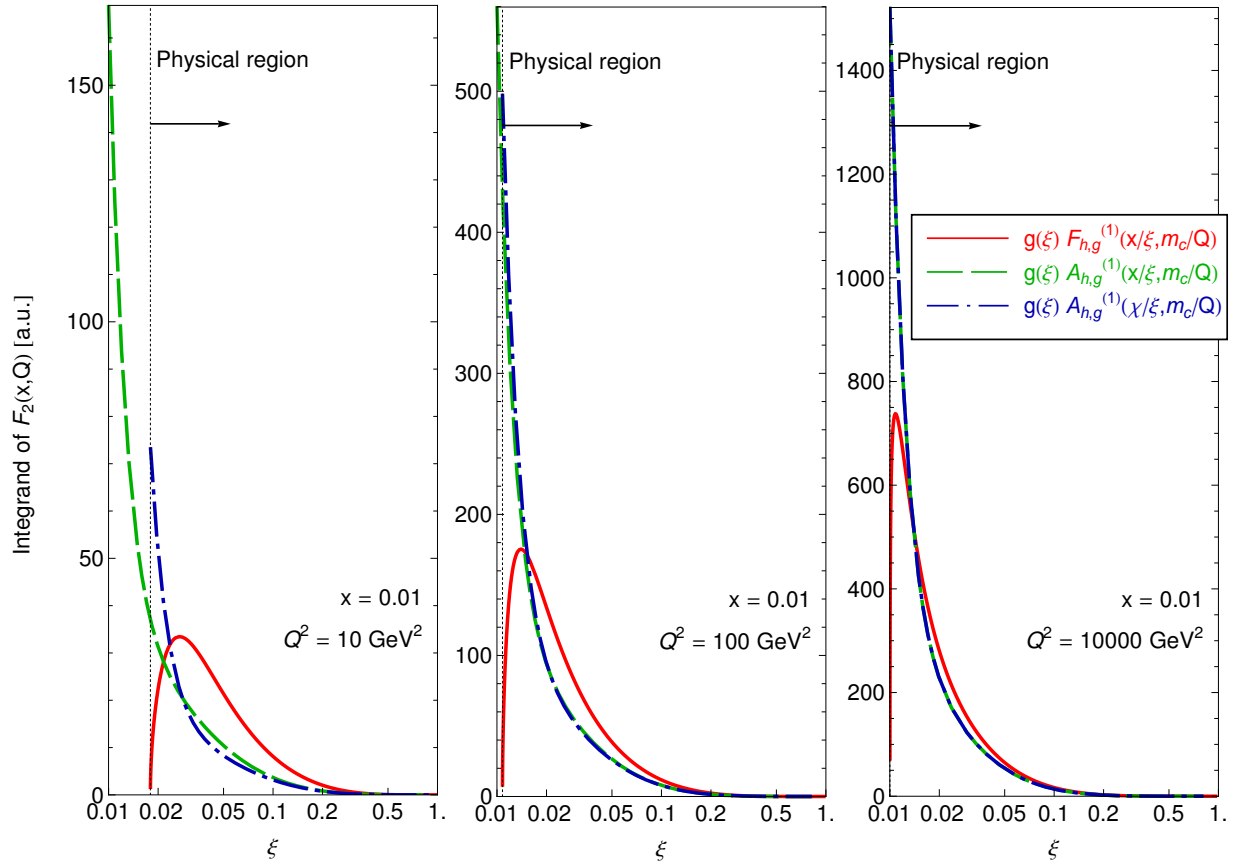
FIG. 4: Integrands of convolution integrals $F_{h,g}^{(1)} \otimes g$ and $A_{h,g}^{(1)} \otimes g$ with and without the χ prescription, plotted as a function of the momentum fraction ξ.

2. The integration over ξ proceeds over the physical range $\chi \leq \xi \leq 1$ in all channels. It includes all physically possible scattering channels for $\xi \geq \chi$, but excludes kinematically prohibited values for $\xi < \chi$. Since the form of χ is associated with a specific coefficient function, the same form is to be used in convolutions of this coefficient function in subtraction terms at higher orders.

3. The S-ACOT-χ coefficient functions H_h in the flavor-excitation channels are given by ZM expressions evaluated at $\hat{x} = \chi/\xi$. Kinematical prefactors outside of the coefficient functions are independent of ξ and not affected by the rescaling.

4. The target subgraphs T_a, corresponding to the PDFs, are given by universal operator matrix elements that are the same in all ACOT-like schemes.

5. The same value N_f is used in the evolution of $\alpha_s(\mu)$, PDFs, and hard graphs in each Q range.

6. When Q is much larger than m_h, the coefficient functions of the S-ACOT-χ scheme reduce to those of the zero-mass $\overline{\text{MS}}$ scheme, without additional finite renormalizations.

7. When Q is of order m_h, the S-ACOT-χ scheme is generally closer to the FFN scheme than the S-ACOT scheme as a consequence of its Z operation that satisfies energy conservation. In this scheme, matching on the FFN scheme does not rely on propositions beyond the factorization theorem with energy conservation, such as conditions for derivatives of $F(x, Q)$ [15] or damping factors [18].

An illustration for the χ convention

The advantages of χ rescaling can be demonstrated on the example of the $\mathcal{O}(\alpha_s)$ $\gamma^* g$ contribution, consisting of the gluon-initiated box graph and corresponding subtraction, and shown by the second and third graphs on the upper row of Fig. 1:

$$[C_{h,g}^{(1)} \otimes g](x, Q) = \int_\chi^1 \frac{d\xi}{\xi} g(\xi, Q) F_{h,g}^{(1)}\left(\frac{\chi}{\xi}\right) - \int_\zeta^1 \frac{d\xi}{\xi} g(\xi, Q) A_{h,g}^{(1)}\left(\frac{\zeta}{\xi}\right). \qquad (50)$$

The integrands of the convolution integrals on the right-hand side, $g(\xi, Q) F_{h,g}^{(1)}(\chi/\xi)$ and $g(\xi, Q) A_{h,g}^{(1)}(\zeta/\xi)$, where $\zeta = x$ or χ, are plotted in Fig. 4(a-c) as a function of ξ. The computation follows the numerical setup described in the next section. The scale on the

ξ axis is logarithmic: the convolution integrals are proportional to the areas under the respective integrand curves. For definiteness, we choose $x = 0.01$ and $Q^2 = 10$, 100, and 10000 GeV^2, but the same features are observed for other x and Q values.

In the charm creation contribution, $g \otimes F_{hg}^{(1)}$, the integrand (red solid line) vanishes outside of the physical range $\chi \leq \xi \leq 1$, where $\chi \approx 0.018$, 0.0108, and 0.010008 for $Q^2 = 10$, 100, and 10000 GeV^2. On the other hand, the naive choice $\zeta = x$ of the S-ACOT scheme allows the integrand $g(\xi, Q) A_{h,g}^{(1)}(\zeta/\xi)$ (green dashed curve) in the second term on the right-hand side of Eq. (50) to contribute in the unphysical region $x \leq \zeta \leq \chi$. Its spurious contribution is comparatively large at the smallest Q. It is not fully canceled by the counterpart FE term $\left[c_{h,h}^{(0)} \otimes c \right](x, Q)$ in the first upper graph of Fig. 1, leading to a bloated higher-order uncertainty.

The S-ACOT-χ integrand $g(\xi, Q) A_{h,g}^{(1)}(\chi/\xi)$ vanishes below $\xi = \chi$ (cf. the blue dash-dotted line). It is numerically moderate at physical ξ values, $\xi > \chi$, and its integral cancels well with $\left[c_{h,h}^{(0)} \otimes c \right](\chi, Q)$, as will be further demonstrated in Sec. IV A. Note also that the difference between the two definitions for the $g(\xi, Q) A_{h,g}^{(1)}(\zeta/\xi)$ integrand is small in most of the physical range $\chi \leq \xi \leq 1$.

As the virtuality Q increases, the difference between χ and x progressively reduces, and ξ varies in a wider interval. Finally in (c), for very large Q, the S-ACOT and S-ACOT-χ subtractions become identical. $A_{h,g}^{(1)} \otimes g$ approximates well the collinear splitting contribution that drives much of the shape of $F_{h,g}^{(1)}(\chi/\xi) g(\xi)$. When $A_{h,g}^{(1)} \otimes g$ is subtracted from $F_{h,g}^{(1)} \otimes g$ as in Eq. (50), it produces a moderate *negative* $\mathcal{O}(\alpha_s)$ contribution, which is further reduced at NNLO. These cancellations are further examined in Sec. IV B.

III.   NUMERICAL EXAMPLES

In this section, we show representative plots from our validation tests for the NNLO inclusive structure functions $F_2(x, Q)$ and $F_L(x, Q)$ computed according to the S-ACOT-χ method. We focus on the partial contributions in which the photon strikes a charm quark, given by $F_h(x, Q)$ in Eq. (12) for $h = c$, and for structure functions $F = F_2$ or F_L. These contributions are referred to as $F_{2c}(x, Q)$ and $F_{Lc}(x, Q)$ in the figures. The same comparisons have been repeated for the bottom-quark functions F_{2b} and F_{Lb}, as well as for the full inclusive functions $F = \sum_{l=1}^{N_l} F_l + \sum_{h=N_l+1}^{N_f^{fs}} F_h$ and alternative values of Bjorken x.

The results of other tests show similar patterns and can be viewed at [54].

NNLO coefficient functions $F_h^{(2)}(x, Q)$ for massive quarks are computed using a program available from [27]. This program tabulates two-loop heavy-quark coefficient functions in a form that allows fast evaluation of convolution integrals in the Q range covered by the experimental data.

The PDFs in all comparisons are obtained by using the Les Houches Accord toy parametrization [55, 56] at the starting scale $Q_0 = m_c = \sqrt{2}$ GeV. Other input parameters are $\alpha_s(Q_0) = 0.36$ and the pole mass m_c.[4] The switching between 3 and 4 flavors happens at $Q = m_c$. The α_s and PDFs are evolved to higher Q values by the HOPPET computer code [57].[5]

A. Q dependence

Fig. 5 examines Q dependence of charm structure functions F_{2c} (left panel) and F_{Lc} (right panel). They are computed to order α_s^2 in all schemes, referred to as "NNLO" by the counting convention for the *inclusive* structure functions considered here. [In predictions for *semi-inclusive* charm production, the $\mathcal{O}(\alpha_s^2)$ cross section in the FFN scheme is often counted as NLO, since the $\mathcal{O}(\alpha_s^0)$ flavor-excitation cross section is absent in this scheme.] The upper insets in both panels show predictions at $x = 10^{-2}$ in the S-ACOT-χ scheme, FFN scheme with $N_f = 3$, and ZM scheme with $N_f = 4$. The lower insets show ratios of the FFN and ZM predictions to the S-ACOT-χ prediction.

The left panel shows that the S-ACOT-χ theory prediction for $F_{2c}(x, Q)$ (blue solid line) is numerically close to the FFN prediction (red short-dashed line) at $Q \approx m_c$ and to the ZM prediction (magenta long-dashed line) at $Q > 10$ GeV.

Similarly, in the right panel, the S-ACOT-χ prediction for the longitudinal function $F_{Lc}(x, Q)$ coincides with the corresponding FFN prediction at $Q \approx m_c$ and approaches the ZM prediction at $Q > 30$ GeV. [$F_{Lc}(x, Q)$ is sensitive to mass-dependent corrections to

---

[4] Our program can alternatively read $\overline{\text{MS}}$ masses as the input. In this case, the $\overline{\text{MS}}$ masses are later converted into the respective pole masses, because the operator matrix elements $A_{ab}^{(k)}$ are published as functions of the pole masses.

[5] Bottom-quark contributions are omitted in this comparison. The charm PDF is zero at $Q < Q_0 = m_c$, but acquires a non-negligible value immediately above Q_0 through an $\mathcal{O}(\alpha_s^2)$ discontinuity existing at the switching point.

scattering off longitudinally polarized photons. Its matching on the ZM prediction happens at higher Q values than in F_{2c}.] The S-ACOT-χ prediction interpolates between the FFN and ZM predictions at intermediate Q values, precisely as expected.
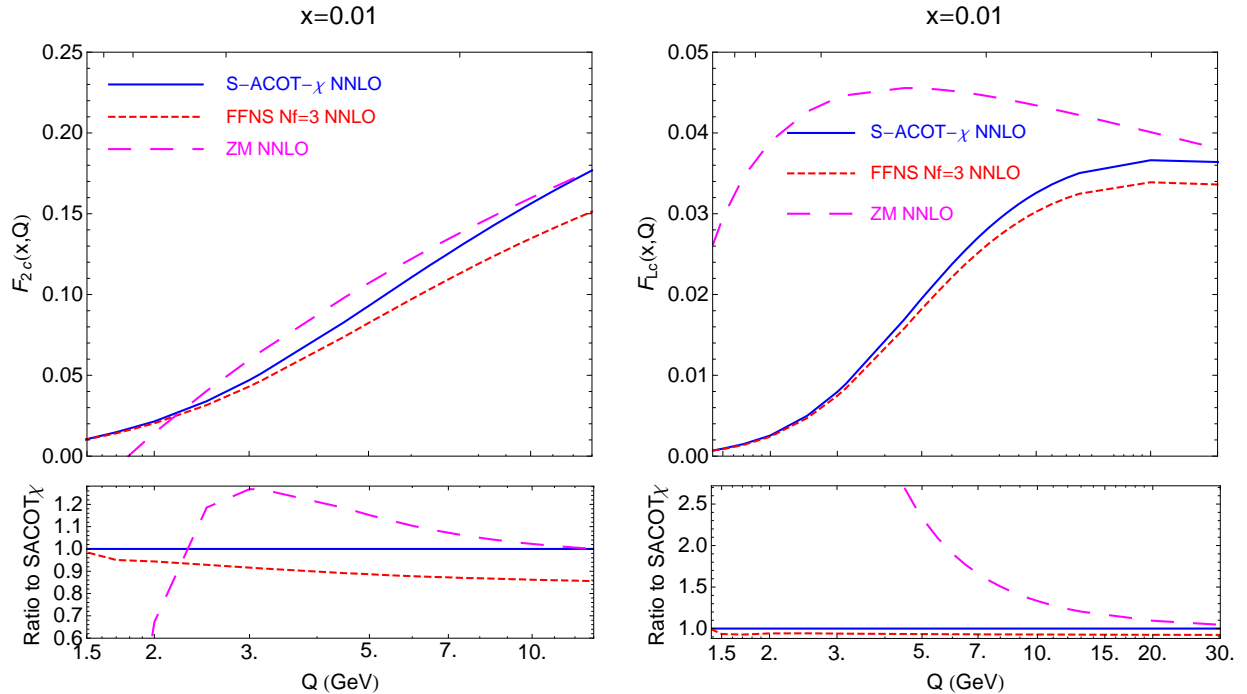

FIG. 5: Comparison of $F_{2c}(x, Q)$ (left) and $F_{Lc}(x, Q)$ (right), computed at $\mathcal{O}(\alpha_s^2)$ in the S-ACOT-χ (solid), FFN $N_f = 3$ (short dashed), and ZM $N_f = 4$ (long dashed) schemes, shown as a function of Q at $x = 10^{-2}$.

B. Dependence on the factorization scale

NLO computations leave substantial uncertainty in the DIS charm-quark contributions due to the choice of the renormalization/factorization scale and differences in the FE terms in the threshold region. NNLO terms drastically reduce these uncertainties. Factorization scale dependence, and its reduction from NLO to NNLO, is illustrated by Fig. 6. Reduction of uncertainties in the modeling of kinematical threshold effects is discussed in Sec. III D.

In Fig. 6(a)-(c), predictions for $F_{2c}(x, Q)$ in the S-ACOT-χ and FFN ($N_f = 3$) schemes are plotted versus Bjorken x at representative Q^2 values of 4, 10, and 100 GeV^2. The $F_{2c}(x, Q)$ values on the y axis are multiplied by $10^3\sqrt{x}$ to better visualize the accessible x region. Central predictions are computed for $\mu = \sqrt{Q^2 + m_c^2}$, the default scale in heavy-
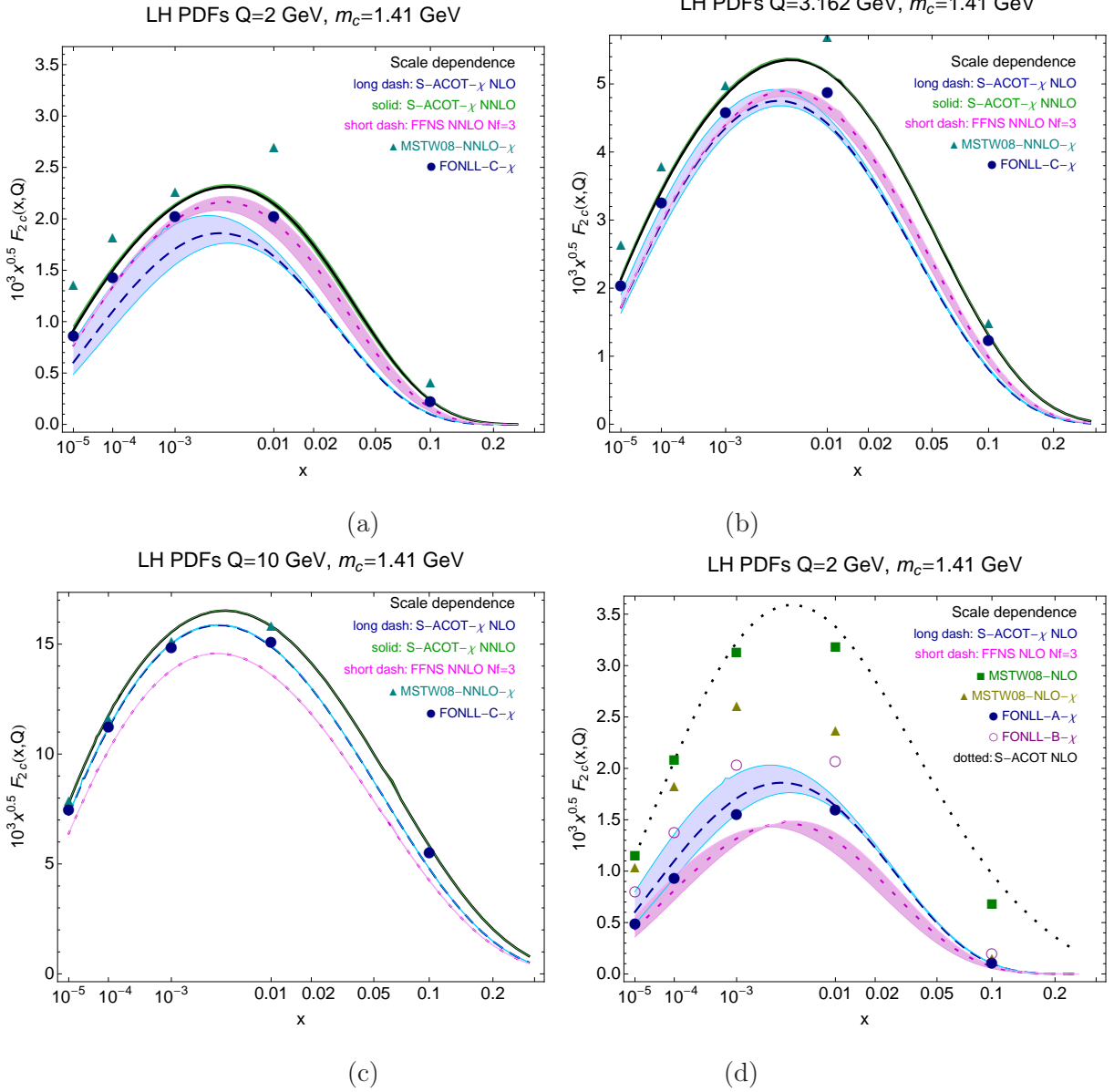
FIG. 6: Comparison of predictions for $F_{2c}(x,Q)$ in the S-ACOT-χ scheme and alternative theoretical approaches at NLO ($O(\alpha_s)$) and NNLO ($O(\alpha_s^2)$). Central predictions are for $\mu = \sqrt{Q^2 + m_c^2}$, and the error bands are for $Q \leq \mu \leq \sqrt{Q^2 + 4m_c^2}$.

quark DIS cross sections in the CT10 global analysis [6]. The error bands are obtained by varying the scale in the range $Q \leq \mu \leq \sqrt{Q^2 + 4m_c^2}$.

At $Q = 2$ GeV in Fig. 6(a), the NNLO S-ACOT-χ central prediction (black solid line inside a green band) is slightly above the NNLO FFN prediction (short-dashed line inside a magenta band) and has a smaller scale uncertainty than FFN. At Q below 2 GeV (not shown), the NNLO S-ACOT-χ and FFN predictions get even closer. In contrast, the NLO S-ACOT-χ prediction (a long-dashed line inside a blue band) underestimates the NNLO FFN result and has wider scale dependence.

As Q increases to 10 GeV (Fig. 6(c)), S-ACOT-χ predicts more event rate than the FFN scheme both at NLO and NNLO. Altogether, the Q dependence in these figures is fully compatible with the matching of the S-ACOT-χ results on the FFN and ZM results in the limits $Q^2 \approx m_c^2$ and $Q^2 \gg m_c^2$, respectively.

C.   NNLO vs. NLO predictions

Improved stability of the NNLO prediction in Fig. 6(a) can be appreciated by comparing it to the counterpart NLO result shown in Fig. 6(d). Here, we collect a variety of NLO $F_{2c}(x, Q)$ values at $Q = 2$ GeV, obtained in FFN, S-ACOT, TR'/MSTW, FONLL-A, and FONLL-B schemes. The S-ACOT and MSTW predictions are shown with the χ scaling as well as without it.

The spread in NLO values of $F_{2c}(x, Q)$ observed in the figure is extensive, nominally suggesting a large uncertainty in the resulting NLO PDF sets. However, when included in the PDF fits, the most extreme predictions for $F_{2c}(x, Q)$ in this figure are excluded by the fitted DIS data, which prefer the values that are about the same as the (relatively unambiguous) NNLO result. In the CT10 NLO fit, the scale μ is set equal to $\sqrt{Q^2 + m_c^2}$, which brings the NLO S-ACOT-χ prediction in agreement with the measured cross sections. Thus, according to the past global fits, the NLO cross sections can be reconciled with the heavy-quark data, but at the expense of tuning of the scale parameter, for each value of m_c and rescaling variable. The key benefit of the NNLO calculation for $F_{2c}(x, Q)$ is to automatically achieve such a good agreement, nearly independently of the factorization scale.
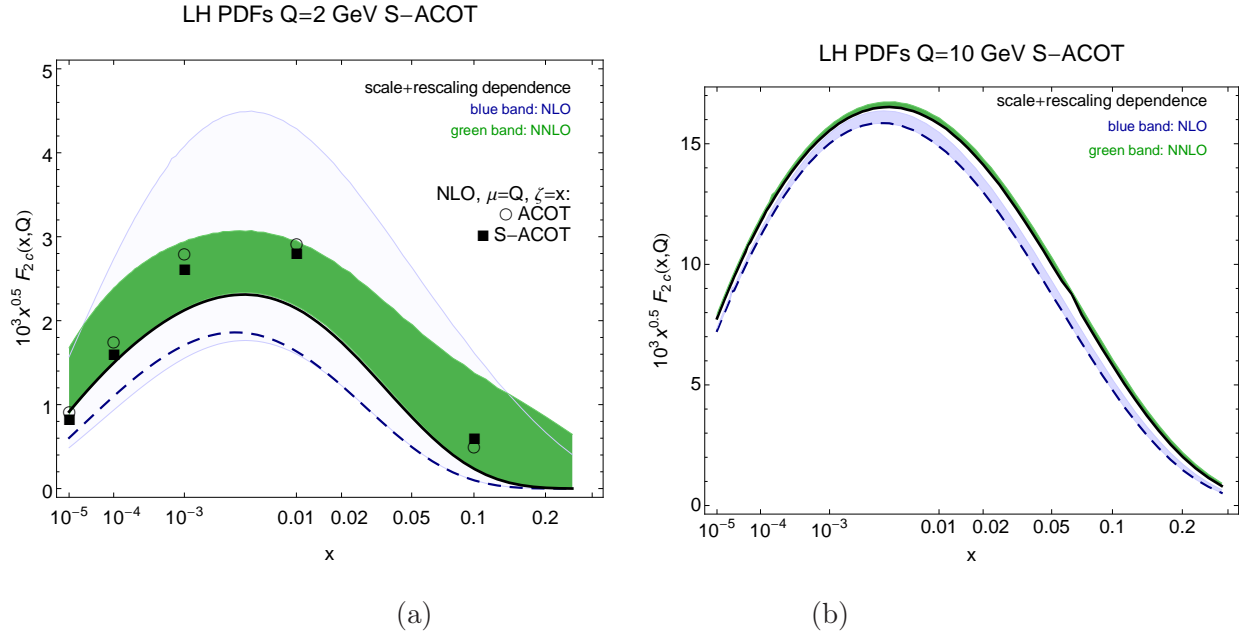
D. Threshold effects

LH PDFs Q=2 GeV S−ACOT

LH PDFs Q=10 GeV S−ACOT

(a)

(b)

FIG. 7: Dependence on the factorization scale μ and the rescaling variable $\zeta(\lambda)$. Left: $Q = 2$ GeV; right: $Q = 10$ GeV.

In the above discussion, our NNLO structure functions are computed using the optimal rescaling variable $\zeta = \chi$ in the FE heavy-quark contributions. The rescaling variable significantly improves convergence near the threshold by excluding contributions to the FE convolution integrals that are kinematically impossible.

Dependence on the rescaling prescription can be explored with the help of the variable ζ that generalizes the χ variable as proposed in Ref. [42]. The generalized rescaling variable ζ is implicitly defined by

$$x = \frac{\zeta}{1 + \zeta^\lambda \cdot (4m_c^2)/Q^2}, \tag{51}$$

where λ is a real number. Various choices of positive λ produce a family of GM schemes in which ζ takes continuous values between x (no rescaling) and χ (full rescaling). Specifically, $\lambda = 0$ produces $\zeta = \chi$ of the S-ACOT-χ scheme, and $\lambda \gg 1$ produces $\zeta \approx x$ that corresponds to the plain S-ACOT scheme without rescaling. Negative λ values (not shown) strongly suppress the FE contributions by setting $\zeta > \chi$.

Fig. 7 shows the bands of variations in the NLO and NNLO S-ACOT F_{2c} values at $Q = 2$ GeV (left panel) and 10 GeV (right panel) when μ and λ are varied in the ranges

$Q \leq \mu \leq \sqrt{Q^2 + 4m_c^2}$ and $0 \leq \lambda \leq 100$, respectively. If λ is naively varied in the full range, at smallest Q values one obtains a large excursion in the NLO predictions (light blue band), which is considerably reduced when going to NNLO (green band).

In contrast to the kinematical dependence on the rescaling variable, the "dynamic" mass terms in the flavor-excitation Wilson coefficients of the "full" ACOT scheme (cf. Section II F) have little effect [4]. The left panel compares the NLO F_{2c} values in the ACOT and S-ACOT schemes for $\mu = Q$ without rescaling from Ref. [58], as indicated by the circles and squares, respectively. The discrepancy between the ACOT and S-ACOT values is small already at NLO. It is likely to further decrease when going to the NNLO as a term of order α_s^3.

As Q increases above a few GeV, dependence on λ diminishes practically to nil, as in the right panel of the figure for $Q = 10$ GeV. The ACOT and S-ACOT scheme produce essentially coinciding predictions at such a large Q value [58]. Together with Fig. 6, Fig. 7 indicates that, at NNLO, the physically motivated rescaling variable is more important at low Q than the factorization scale choice or the difference between the ACOT and S-ACOT schemes.

E. Alternative mass schemes

1. TR' and FONLL schemes

Figs. 6(a)-(c) also show NNLO predictions in alternative GM schemes, indicated by scattered symbols: the modified Thorne-Roberts (TR') scheme [14–16] as implemented by the MSTW'08 PDF analysis [59]; and FONLL scheme C used by the NNPDF collaboration [18]. Their values are computed in the 2009 Les Houches benchmark study of GM schemes [58] by assuming the same χ rescaling as the S-ACOT-χ scheme.

The three schemes are seen to be in good overall agreement, apart from minor differences traced to subtle variations in the NNLO implementations that the schemes provide.

At $Q = 2$ GeV, the NNLO S-ACOT-χ prediction lies slightly above the FONLL-C prediction and below the MSTW prediction. At $Q = 10$ GeV, the NNLO S-ACOT-χ prediction becomes closer to the MSTW prediction and is still above the FONLL-C result. These differences can be understood by noticing that the compared schemes may differ in subleading perturbative terms. For example, the FONLL-C scheme includes a threshold damping fac-

tor to match on the 3-flavor result near the threshold [18]. The S-ACOT-χ scheme is not using the damping factor and is expectedly close to the FONLL-C scheme at $Q \to m_c$, but not strictly identical. The TR'/MSTW prediction includes a constant higher-order term (of order $\mathcal{O}(\alpha_s^3)$) to improve smoothness of switching from 3 to 4 flavors at $Q = m_c$. Neither S-ACOT-χ nor FONLL-C include this artificial constant term, which is why they may predict smaller F_{2c} values at low Q.

2. The BMSN scheme

Structural similarities between the S-ACOT-χ, TR', and FONLL schemes reflect their conceptual origin from the Collins-Wilczek-Zee (CWZ) renormalization method [60]. The CWZ procedure is applied frequently to renormalize QCD quantities dependent on several mass scales. It introduces a sequence of renormalization schemes and associated differential equations with the number N_f of active flavors that changes across particle mass thresholds. The CWZ procedure is invoked, for example, in the common definition of the QCD running coupling α_s and by the zero-mass VFN scheme.

The family trait of the CWZ renormalization – a hierarchy of fixed-flavor number sub-schemes with sequentially incrementing N_f values – is also evident in the ACOT-like general mass schemes. In practical realizations of these schemes, scale dependence of *both* α_s and PDFs is found by solving renormalization group equations with a shared N_f value in each mass range. The N_f and $N_f + 1$ expressions for α_s and PDFs are related at the switching momentum scales through the known matching conditions.

A different path is taken in the approach of Buza, Matiuonine, Smith, and van Neerven (BMSN [12]), which is adopted, for example, in the fits by the ABM group [17, 61]. In the BMSN and CSN [13] frameworks, only $\alpha_s(\mu)$ is found from a renormalization group equation according to the CWZ procedure. However the 4-flavor PDFs are *constructed* from the 3-flavor PDFs at $\mu \geq m_c$ by solving the matching equations for each μ value. Only the 3-flavor PDFs are evolved by the DGLAP equations in this case. Here we see the key difference with the ACOT approach, which resums higher-order corrections to the heavy-flavor PDFs at $\mu \geq m_c$ with the help of DGLAP equations. The BMSN method does not provide this resummation, crucial for implementing the precise collider data from $Q^2 \gg m_c^2, m_b^2$ into the global fit. To resum the heavy-quark collinear logs in their published 5-flavor PDFs,

ABM evolve them from the initial scale m_b to higher energies *after* the fit, starting from the best-fit parametrization found in the BMSN approach.

In the BMSN framework, the number N_f of active quark flavors in α_s is incremented from 3 to 5 according to the usual convention as the energy increases. 4-flavor PDFs $f_a(4, x, \mu^2)$ are derived from the 3-flavor PDFs $f_a(3, x, \mu^2)$ as

$$f_a(4, x, \mu^2) = \sum_b [A_{ab} \otimes f_b](3, x, \mu^2); \tag{52}$$

The functions $A_{ab}(\widehat{x}) = \delta_{ab}\delta(1-\widehat{x}) + a_s A_{ab}^{(1)}(\widehat{x}) + a_s^2 A_{ab}^{(2)}(\widehat{x}) + ...$ are comprised of the coefficients $A_{ab}^{(k)}$ in the perturbative expansion of the massive parton-level PDFs that were discussed in Sec. II A. The BMSN 4-flavor structure function is given by

$$F^{BMSN}(4, x, Q) = F(3, x, Q, m_c \neq 0) + F(4, x, Q, m_c = 0) - F^{asymp}(3, x, Q, m_c \neq 0), \tag{53}$$

where $F(3, x, Q, m_c \neq 0)$ is obtained for three massless quarks (u, d, s) and one massive quark (c). $F^{asymp}(3, x, Q, m_c \neq 0)$ is the dominant part of $F(3, x, Q, m_c \neq 0)$ in the asymptotic limit $Q^2 \gg m_c^2$, and $F(4, x, Q, m_c = 0)$ is computed with 4 massless quarks in the Wilson coefficients, with the 4-flavor PDFs defined by Eq. (52).

This arrangement provides a nearly ideal matching of the 4-flavor $F^{BMSN}(4, x, Q)$ onto the 3-flavor $F(3, x, Q, m_c \neq 0)$ as $\mu \to m_c$, which is feasible in the absence of resummation of collinear logs $\ln(\mu^2/m_c^2)$. At $\mathcal{O}(\alpha_s^2)$, the last two terms in Eq. (53) are related by the replacement of the 3-flavor QCD coupling by the 4-flavor coupling,

$$F(4, x, Q, m_c = 0) = \left(F^{asymp}(3, x, Q, m_c \neq 0) \right)_{\alpha_s(3,\mu) \to \alpha_s(4,\mu) - \frac{1}{6\pi}\alpha_s^2 \ln\left(\frac{\mu^2}{m_h^2}\right)} . \tag{54}$$

Since $\alpha_s(N_f, \mu)$ is nearly continuous at the switching point between 3 and 4 flavors (apart from a mild discontinuity that first enters at $\mathcal{O}(\alpha_s^2)$), it follows from Eqs. (53) and (54) that $F^{BMSN}(4, x, Q) \approx F(3, x, Q, m_c \neq 0)$ at $Q \to m_c$. In a nutshell, the matching of the BMSN 4-flavor scheme on the 3-flavor scheme is achieved by dropping the numerical DGLAP evolution of 4-flavor PDFs.

In deriving these relations, BMSN allow only *one* parton flavor to be massive in each μ range. This assumption is untrue at some level for μ comparable to m_b, since m_c is not negligible compared to m_b. It creates conceptual difficulties in extending the VFN scheme proposed by BMSN to three loops [36, 37], since both the parton-level structure functions $F_{a,b}^{(3)}$ and operator matrix elements $A_{ab}^{(k)}$ may depend on m_c and m_b at the same time.

In fact, this assumption is not necessary for proving QCD factorization with heavy quarks and is not made in the S-ACOT approach. The proof of the general-mass factorization scheme does not need to assume that all quarks but one are massless. Masses of heavy quarks that may be comparable to Q are never neglected in the target subgraphs associated with the PDFs and $A_{ab}^{(k)}$, cf. Ref. [3] and Sec. II F. As an illustration of their role, consider again the coefficient function $C_{b,g}^{(3)}$ with c and b quark lines in Eq. (41) of Sec. II D. This function is found by subtracting convolutions of massive operator matrix elements $A_{bg}^{(k)}$ from a massive parton-level function $F_{b,g}^{(3)}$. This is expected to produce $C_{b,g}^{(3)}$ that is free of the $\ln(\mu^2/m_c^2)$ and $\ln(\mu^2/m_b^2)$ terms and coincides with $C_{b,g}^{(3)}$ in the effective $\overline{MS}$ scheme with 5 massless flavors when Q^2 is unequivocally larger than m_c^2 and m_b^2. [Verification of this prediction still awaits an explicit calculation of the massive function $F_{b,g}^{(3)}$]. The operator matrix element $A_{bg}^{(3)}$ that depends both on m_c and m_b, and which caused concern in Refs. [36, 37], therefore naturally appears in the factorization formula (41) when deriving the infrared-safe $C_{b,g}^{'(3)}$ with two quark species. It is not anticipated to pose a problem from the S-ACOT-χ viewpoint.

Numerically, the S-ACOT-χ and BMSN approaches provide close predictions for charm production at $Q \approx m_c$ [58]. While both approaches are in good agreement with the current HERA data, they may lead to numerical differences in future precise DIS analyses, both at scales of order m_b, where the resummed $\ln(Q^2/m_c^2)$ terms may already play some role, and at electroweak scales, where the expected differences of a few percent may be comparable to the PDF uncertainties. More generally, S-ACOT-χ points out a way to include heavy-quark mass dependence and resummation of heavy-quark collinear logs in one step, and to implement three-loop DIS amplitudes with two massive quark flavors along the guidelines of the CWZ renormalization.

IV.   CANCELLATIONS BETWEEN FEYNMAN GRAPHS

A.   Cancellations at low Q

In order to match on the FFN and ZM predictions, certain classes of Feynman diagrams inside the S-ACOT-χ NNLO coefficient functions must cancel in the respective low-Q and large-Q regions. We will show how these cancellations come about in the case of the charm-quark function $F_{2c}(x, Q)$, but the pattern holds for the bottom quark and other structure

functions with suitable modifications.

The cancellations are revealed by plotting differences between various matrix elements and collinear subtractions discussed in Section II A, which are established by applying the factorization formula at the parton level.

In the $Q \approx m_c$ region, all FE contributions in Eqs. (18)-(21) must cancel to a high degree in order for $F_{2c}(x, Q)$ to reduce to the FFN matrix elements $F_{h,g}^{(1,2)}$ and $F_{h,l}^{(2)}$. In the threshold region, the evolved charm PDF is effectively of order $\mathcal{O}(a_s)$,

$$\lim_{Q^2 \to m_c^2} c(x, Q) \approx a_s(Q) \left[A_{hg}^{(1)} \otimes g \right] (x, Q); \tag{55}$$

a FE contribution to $F_{2c}(x, Q)$ containing a coefficient $c_{h,h}^{(k)}$ is effectively of order $\mathcal{O}(a_s^{k+1})$. Keeping this in mind, at order $\mathcal{O}(a_s)$ the virtual-photon-charm scattering diagram with $c_{h,h}^{(0)}$ in Eq. (18) cancels the gluon-initiated subtraction term with $A_{hg}^{(1)}$ in Eq. (19), and only the $\gamma^* g$ fusion diagram $F_{hg}^{(1)}$ in Eq. (19) survives in the total $F_{2c}(x, Q)$. In this case, the difference

$$D_{C^{(0)}}^{(1)}(x, Q) = \left[c_{h,h}^{(0)} \otimes c \right] (x, Q) - a_s \left[c_{h,h}^{(0)} \otimes A_{hg}^{(1)} \otimes g \right] (x, Q), \tag{56}$$

where $c(x, Q)$ and $g(x, Q)$ represent the charm and gluon PDFs, must be close to zero.

As the next order is included, the cancellation present in $D_{C^{(0)}}^{(1)}$ must further improve. Two differences quantify the cancellations to this order:

$$D_{C^{(0)}}^{(2)}(x, Q) = D_{C^{(0)}}^{(1)}(x, Q) - a_s^2 \left[c_{h,h}^{(0)} \otimes A_{hg}^{(2)} \otimes g \right] (x, Q) - a_s^2 \left[c_{h,h}^{(0)} \otimes A_{hl}^{PS,(2)} \otimes \Sigma \right] (x, Q), \tag{57}$$

in which the convolutions of $c_{h,h}^{(0)}$ with $O(\alpha_s^2)$ operator matrix elements $A_{hg}^{(2)}$ and $A_{hl}^{PS,(2)}$ are subtracted from $D_{C^{(0)}}^{(1)}(x, Q)$; and

$$D_{C^{(1)}}^{(2)}(x, Q) = a_s \left[c_{h,h}^{(1)} \otimes c \right] (x, Q) - a_s^2 \left[c_{h,h}^{(1)} \otimes A_{hg}^{(1)} \otimes g \right] (x, Q), \tag{58}$$

which probes the cancellation between convolutions involving the coefficient $c_{h,h}^{(1)}$. By comparing $D_{C^{(0)}}^{(2)}$ with $D_{C^{(0)}}^{(1)}$, we quantify how the $\mathcal{O}(a_s)$ cancellation in $D_{C^{(0)}}^{(1)}$, proportional to $c_{h,h}^{(0)}$, improves upon the inclusion of the NNLO corrections. The difference $D_{C^{(1)}}^{(2)}$ quantifies yet another $\mathcal{O}(a_s^2)$ cancellation that is independent of $D_{C^{(0)}}^{(1)}$. It has the same structure as $D_{C^{(0)}}^{(1)}$, but includes the convolutions with $c_{h,h}^{(1)}$ instead of $c_{h,h}^{(0)}$.

The left panel of Fig. 8 shows the x dependence of $D_{C^{(0)}}^{(1)}$, $D_{C^{(0)}}^{(2)}$, and $D_{C^{(1)}}^{(2)}$ at $Q = 2$ GeV. To provide visual guidance, these differences are compared to the FFN $N_f = 3$ prediction at $\mathcal{O}(a_s^2)$ (solid black line), which is roughly equal to the total rate at this Q (cf. the previous

subsection). We also plot the S-ACOT-χ contribution of $\mathcal{O}(a_s^0)$ provided by $c_{h,h}^{(0)}$ (dashed blue line), nominally counted as the lowest-order contribution. While the LO contribution on its own is substantial comparatively to the FFN result, it is mostly canceled by the subtraction in Eq. (56), so that the resulting difference $D_{C^{(0)}}^{(1)}$ (long-dashed green line) is small.

The cancellation in $D_{C^{(0)}}^{(1)}$ is further improved by including the next-order terms in $D_{C^{(0)}}^{(2)}$ as in Eq. (57). The difference $D_{C^{(0)}}^{(2)}$ (dot-dashed red line) and especially the counterpart difference $D_{C^{(1)}}^{(2)}$ (dotted purple line) give decreasingly small contributions. They satisfy

$$\left| D_{C^{(1)}}^{(2)} \right| \ll \left| D_{C^{(0)}}^{(2)} \right| \ll \left| D_{C^{(0)}}^{(1)} \right| \leq F_{2,c}(x, Q). \tag{59}$$

Therefore, as $Q \to m_c$, the S-ACOT-χ scheme exhibits an almost perfect match on the FFN computation by the virtue of perturbative cancellations that improve with each order of α_s.
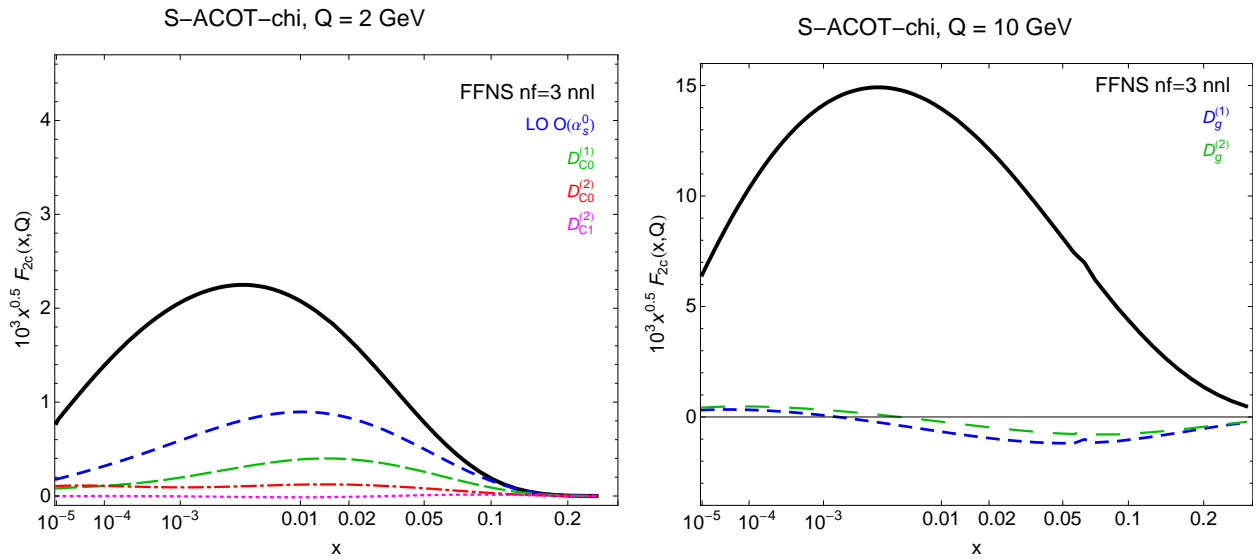

FIG. 8: Cancellations in the S-ACOT-χ scheme at $Q^2 \approx m_c^2$ (left) and $Q^2 \gg m_c^2$ (right).

B. Cancellations at large Q

A different cancellation pattern is observed when m_c is negligible compared to Q, when the large logarithms collected in $A_{hg}^{(1)}$, etc. must be subtracted from the massive contributions $F^{(k)}$ to obtain the infrared-safe coefficient functions $C^{(k)}$. These cancellations are illustrated in the right panel of Fig. 8 by $D_g^{(1)}$ and $D_g^{(2)}$. They quantify the collinear subtractions in the

contributions containing the $\gamma^* g$ box subgraph. The lowest-order difference $D_g^{(1)}$ is equal to the convolution of the coefficient $C_{h,g}^{(1)}$ as defined by Eq.(19):

$$D_g^{(1)}(x, Q) \equiv \left[C_{h,g}^{(1)} \otimes g \right](x, Q) = a_s \left\{ \left[F_{h,g}^{(1)} \otimes g \right](x, Q) - \left[c_{h,h}^{(0)} \otimes A_{hg}^{(1)} \otimes g \right](x, Q) \right\}. \quad (60)$$

In this expression the subtraction term matches on the $\mathcal{O}(a_s)$ photon-gluon contribution represented by $F_{h,g}^{(1)}$. The x dependence of this matching is shown in the right panel of Fig. 8 for $Q = 10$ GeV. It can be seen that $D_g^{(1)}$ (blue short-dashed line) is quite small compared to the $\mathcal{O}(a_s^2)$ FFN result.

The α_s^2-order difference can be constructed as

$$D_g^{(2)}(x, Q) = D_g^{(1)}(x, Q) + a_s^2 \left\{ \left[C_{h,g}^{(2)} \otimes g \right](x, Q) + \left[C_{h,l}^{(2)} \otimes \Sigma \right](x, Q) \right\},$$

which can be cast into the form

$$D_g^{(2)} = D_g^{(1)} + a_s^2 \left\{ \widehat{F}_{h,g}^{(2)} \otimes g + \widehat{F}_{h,l}^{PS,(2)} \otimes \Sigma - c_{h,h}^{(1)} \otimes A_{hg}^{(1)} \otimes g \right.$$
$$\left. - c_{h,h}^{(0)} \otimes A_{hg}^{(2)} \otimes g - c_{h,h}^{(0)} \otimes A_{hl}^{PS,(2)} \otimes \Sigma \right\} \quad (61)$$

by virtue of Eqs. (20) and (21). At this order, the collinear logarithms arising in $\widehat{F}_{h,g}^{(2)}$ are canceled by $c_{h,h}^{(0)} \otimes A_{hg}^{(2)}$ and $c_{h,h}^{(1)} \otimes A_{hg}^{(1)}$, and, similarly, the collinear term in $\widehat{F}_{h,l}^{PS,(2)}$ is removed by $c_{h,h}^{(0)} \otimes A_{hl}^{PS,(2)}$. The net effect of the subtractions is that $D_g^{(2)}$ (the green long-dashed line) provides a small correction to $D_g^{(1)}$. The perturbative series converge well for $D_g^{(k)}$:

$$\left| D_g^{(2)} - D_g^{(1)} \right| \ll \left| D_g^{(1)} \right| \ll F_2^c(x, Q). \quad (62)$$

C.   Cancellations without kinematic rescaling

Although the cancellations happen for any rescaling variable ζ, their perturbative convergence is slower for a non-optimal choice, such as $\zeta = x$. The differences $D_{C^{(0)}}^{(1)}$, etc. for $\zeta = x$ are shown in Fig. 9 and, as one can see, they are generally larger than in the case of $\zeta = \chi$. Nonetheless, the differences are reduced by going to NNLO, although not as fast as for the optimal rescaling choice.
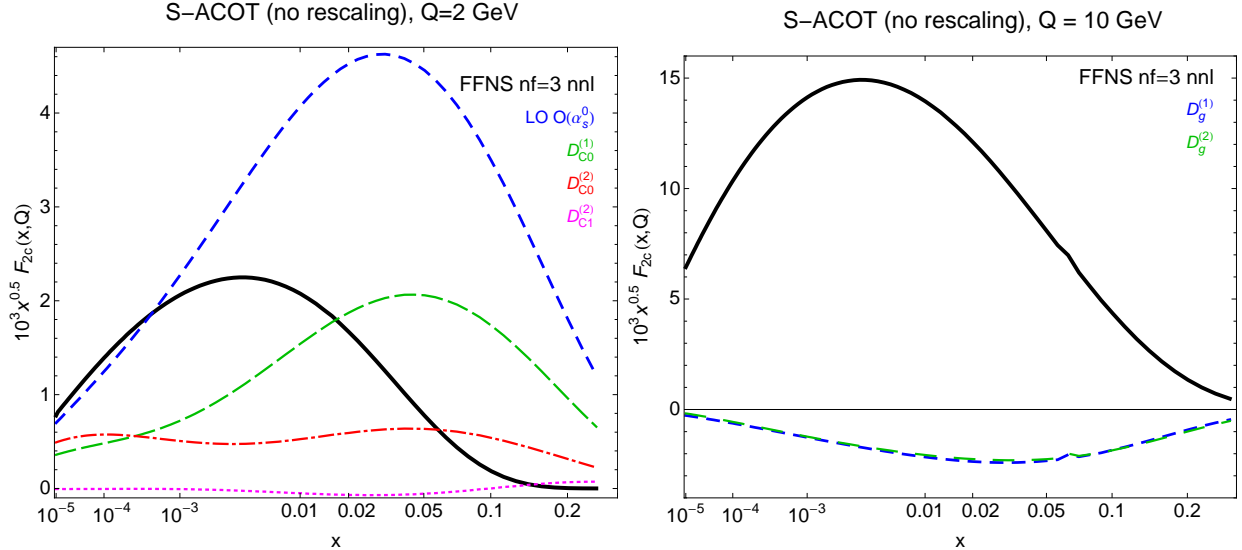
FIG. 9: Same as Fig. 8, in the S-ACOT scheme without rescaling.

V. CONCLUSIONS

We examined connections between multi-loop calculations for massive quark production and fundamental concepts behind QCD factorization. An NNLO calculation for neutral-current DIS with massive quarks is documented in a form that bears structural similarity to the NNLO computation in the zero-mass scheme [19–21]. This calculation is algorithmic and utilizes readily available NNLO expressions. The main formulas are presented by Eqs. (40), (24), and (39). The theoretical derivation presented in Sec. II can be readily extended to two-loops in charged-current DIS, after all needed heavy-quark matrix elements are computed.

The conceptual foundation for the presented results is provided by the S-ACOT-χ factorization scheme. The discussion emphasized several strong features of this scheme: its direct origin from the proof of QCD factorization for DIS [3], relative simplicity, and compliance with phase space constraints on heavy-quark production at all energies.

Throughout this study, we highlighted phenomenological importance of energy conservation in massive particle production. We have shown how the constraints from energy conservation can be satisfied in all channels as a part of the QCD factorization theorem. These constraints are included in the definition of the Z operation in the Collins' proof of QCD factorization by rescaling the partonic momentum fraction in flavor-excitation Wilson coefficients. The rescaling variable depends on the mass $\sum m_h$ of heavy particles in the

final state as $\chi = x \left(1 + (\sum m_h)^2/Q^2 \right)$, where $\sum m_h = 2\,m_h$ and m_h at the lowest order in neutral-current DIS and charged-current DIS, respectively. The S-ACOT-χ scheme thus realizes correct kinematical dependence solely by the means of the QCD factorization theorem and momentum conservation.

Schemes of the ACOT family differ only in mass-dependent terms in heavy-quark Wilson coefficient functions. PDFs are given by the same operator matrix elements in all schemes, such as Eq. (3). Estimates of these PDFs from global fits converge to unique universal functions as order of the QCD coupling increases. Convergence is the fastest in the S-ACOT-χ scheme.

At NNLO, dependence of S-ACOT-χ predictions on the factorization scale and other tunable parameters is reduced compared to NLO. Cancellations between classes of Feynman diagrams are stabilized once NNLO terms are included.

After the first version of this paper has been submitted, an independent S-ACOT-χ calculation for NC DIS has been realized in Ref. [62]. In that approach, full mass dependence is included at $\mathcal{O}(\alpha_s)$, while *approximate* matrix elements are used in all heavy-quark channels at $\mathcal{O}(\alpha_s^2)$ and $\mathcal{O}(\alpha_s^3)$. They are obtained from ZM matrix elements evaluated with a rescaling variable that mimic the dominant kinematic contributions, in an approach that resembles the "intermediate-mass" scheme proposed in Ref. [42]. In our study, the $\mathcal{O}(\alpha_s^2)$ contributions to flavor-creation channels and threshold matching coefficients are computed exactly, so that it reduces to the FFN scheme at $Q \approx m_c$. Since the kinematical mass terms dominate over the dynamical terms in most practical situations [42], the calculation in Ref. [62] is beneficial for obtaining estimates of yet unknown heavy-quark coefficient functions, notably for heavy-quark contributions to neutral-current DIS at three loops and charged-current DIS at two loops.

The derivation of S-ACOT-χ predictions is simpler than in some other GM schemes [12, 29], as it is carried out by assuming a unique number of active flavors (N_f) and one set of universal PDFs in every Q range. It is minimal, in the sense that it does not impose conditions on the Q derivatives of structure functions [14] or introduce a damping factor [18]. Yet, after the NNLO terms are included, the S-ACOT-χ predictions result in good agreement with the other GM schemes. As the default heavy-quark scheme of CTEQ PDF analyses, the S-ACOT-χ scheme is going to play a crucial role in global fits at NNLO.

Acknowledgments

---

[1] W. K. Tung et al., JHEP **02**, 053 (2007).

[2] M. A. G. Aivazis, J. C. Collins, F. I. Olness, and W.-K. Tung, Phys. Rev. **D50**, 3102 (1994).

[3] J. C. Collins, Phys. Rev. **D58**, 094002 (1998).

[4] M. Kramer, 1, F. I. Olness, and D. E. Soper, Phys. Rev. **D62**, 096007 (2000).

[5] W.-K. Tung, S. Kretzer, and C. Schmidt, J. Phys. **G28**, 983 (2002).

[6] H.-L. Lai et al., Phys. Rev. **D82**, 074024 (2010).

[7] P. M. Nadolsky et al., Phys. Rev. **D78**, 013004 (2008).

[8] J. Pumplin et al., Phys. Rev. **D80**, 014019 (2009).

[9] S. Moch and M. Rogal, Nucl.Phys. **B782**, 51 (2007).

[10] S. Moch, J. Vermaseren, and A. Vogt, Nucl.Phys. **B813**, 220 (2009).

[11] M. Buza and W. van Neerven, Nucl.Phys. **B500**, 301 (1997).

[12] M. Buza, Y. Matiounine, J. Smith, and W. L. van Neerven, Eur. Phys. J. **C1**, 301 (1998).

[13] A. Chuvakin, J. Smith, and W. L. van Neerven, Phys. Rev. **D61**, 096004 (2000).

[14] R. S. Thorne and R. G. Roberts, Phys. Lett. **B421**, 303 (1998).

[15] R. S. Thorne and R. G. Roberts, Phys. Rev. **D57**, 6871 (1998).

[16] R. S. Thorne, Phys. Rev. **D73**, 054019 (2006).

[17] S. Alekhin, J. Blümlein, S. Klein, and S. Moch, Phys. Rev. **D81**, 014032 (2010).

[18] S. Forte, E. Laenen, P. Nason, and J. Rojo, Nucl. Phys. **B834**, 116 (2010).

[19] J. Sanchez Guillen, J. Miramontes, M. Miramontes, G. Parente, and O. A. Sampayo, Nucl. Phys. **B353**, 337 (1991).

[20] W. L. van Neerven and E. B. Zijlstra, Phys. Lett. **B272**, 127 (1991).

[21] E. B. Zijlstra and W. L. van Neerven, Phys. Lett. **B273**, 476 (1991).

[22] R. Thorne, PoS **DIS2010**, 053 (2010).

[23] S. Alekhin, S. Alioli, R. D. Ball, V. Bertone, J. Blümlein, et al. (2011), arXiv:1101.0536.

[24] R. Plačakytė (2010), talk at the PDF4LHC meeting, http://indico.cern.ch/materialDisplay.py?contribId=6&sessionId=2&materialId=slides&confId=103872.

[25] F. Aaron et al. (H1 and ZEUS Collaboration), JHEP **1001**, 109 (2010).

[26] E. Laenen, S. Riemersma, J. Smith, and W. L. van Neerven, Nucl. Phys. **B392**, 162 (1993).

[27] S. Riemersma, J. Smith, and W. L. van Neerven, Phys. Lett. **B347**, 143 (1995).

[28] B. Harris and J. Smith, Nucl.Phys. **B452**, 109 (1995).

[29] M. Buza, Y. Matiounine, J. Smith, and W. van Neerven, Phys.Lett. **B411**, 211 (1997).

[30] I. Bierenbaum, J. Blümlein, and S. Klein, Nucl.Phys. **B780**, 40 (2007).

[31] I. Bierenbaum, J. Blümlein, and S. Klein, Phys.Lett. **B672**, 401 (2009).

[32] J. Blümlein, A. De Freitas, W. van Neerven, and S. Klein, Nucl.Phys. **B755**, 272 (2006).

[33] I. Bierenbaum, J. Blümlein, and S. Klein, Nucl.Phys. **B820**, 417 (2009).

[34] J. Ablinger, J. Blümlein, S. Klein, C. Schneider, and F. Wissbrock, Nucl.Phys. **B844**, 26 (2011).

[35] J. Blümlein, A. Hasselhuhn, S. Klein, and C. Schneider (2012), arXiv:1205.4184.

[36] J. Ablinger, J. Blümlein, S. Klein, C. Schneider, and F. Wissbrock (2011), arXiv:1106.5937.

[37] J. Ablinger, J. Blümlein, A. Hasselhuhn, S. Klein, C. Schneider, et al. (2012), arXiv:1202.2700.

[38] E. Laenen and S.-O. Moch, Phys.Rev. **D59**, 034027 (1999).

[39] H. Kawamura, N. L. Presti, S. Moch, and A. Vogt (2012), arXiv:1205.5727.

[40] M. A. G. Aivazis, F. I. Olness, and W.-K. Tung, Phys. Rev. **D50**, 3085 (1994).

[41] R. M. Barnett, Phys.Rev.Lett. **36**, 1163 (1976).

[42] P. M. Nadolsky and W.-K. Tung, Phys. Rev. **D79**, 113014 (2009).

[43] E. Witten, Nucl. Phys. **B104**, 445 (1976).

[44] S. Moch, J. A. M. Vermaseren, and A. Vogt, Phys. Lett. **B606**, 123 (2005).

[45] J. Vermaseren, A. Vogt, and S. Moch, Nucl.Phys. **B724**, 3 (2005).

[46] W. A. Bardeen, A. J. Buras, D. W. Duke, and T. Muta, Phys. Rev. **D18**, 3998 (1978).

[47] G. Altarelli, R. K. Ellis, and G. Martinelli, Nucl. Phys. **B143**, 521 (1978).

[48] B. Humpert and W. L. van Neerven, Nucl. Phys. **B184**, 225 (1981).

[49] M. Buza, Y. Matiounine, J. Smith, R. Migneron, and W. van Neerven, Nucl.Phys. **B472**, 611 (1996).

[50] S. L. Adler, Phys. Rev. **143**, 1144 (1966).

[51] G. Altarelli, Phys. Rept. **81**, 1 (1982).

[52] Y. L. Dokshitzer, G. Marchesini, and B. R. Webber, Nucl. Phys. **B469**, 93 (1996).

[53] R. Brock et al. (CTEQ), Rev. Mod. Phys. **67**, 157 (1995).

[54] M. Guzzi and P. Nadolsky (2010), http://hep.pa.msu.edu/cteq/public/SACOTNNLO2011/.

[55] W. Giele et al. (2002), hep-ph/0204316.

[56] M. R. Whalley, D. Bourilkov, and R. C. Group (2005), hep-ph/0508110; http://hepforge.cedar.ac.uk/lhapdf/.

[57] G. P. Salam and J. Rojo, Comput. Phys. Commun. **180**, 120 (2009).

[58] J. Rojo, S. Forte, J. Huston, P. Nadolsky, P. Nason, F. Olness, R. Thorne, and G. Watt (SM and NLO Multileg Working Group) (2010), p. 110, arXiv:1003.1241.

[59] A. D. Martin, W. J. Stirling, R. S. Thorne, and G. Watt, Eur. Phys. J. **C63**, 189 (2009).

[60] J. C. Collins, F. Wilczek, and A. Zee, Phys.Rev. **D18**, 242 (1978).

[61] S. Alekhin, J. Blümlein, and S. Moch (2012), arXiv:1202.2281.

[62] T. Stavreva, F. Olness, I. Schienbein, T. Jezo, A. Kusina, et al. (2012), arXiv:1203.0282.